AD-A062 078 CASE WESTERN RESERVE UNIV CLEVELAND OH PLASMA RESEAR--ETC F/G 10/3
THEORETICAL AND EXPERIMENTAL STUDY OF SUPERCONDUCTING INDUCTIVE--ETC(U)
OCT 78 O K MAWARDI, D HAZONY, H K CHUNG AFOSR-76-2886

UNCLASSIFIED AFOSR-TR-78-1500 NL

1 OF 2
ADA
062078

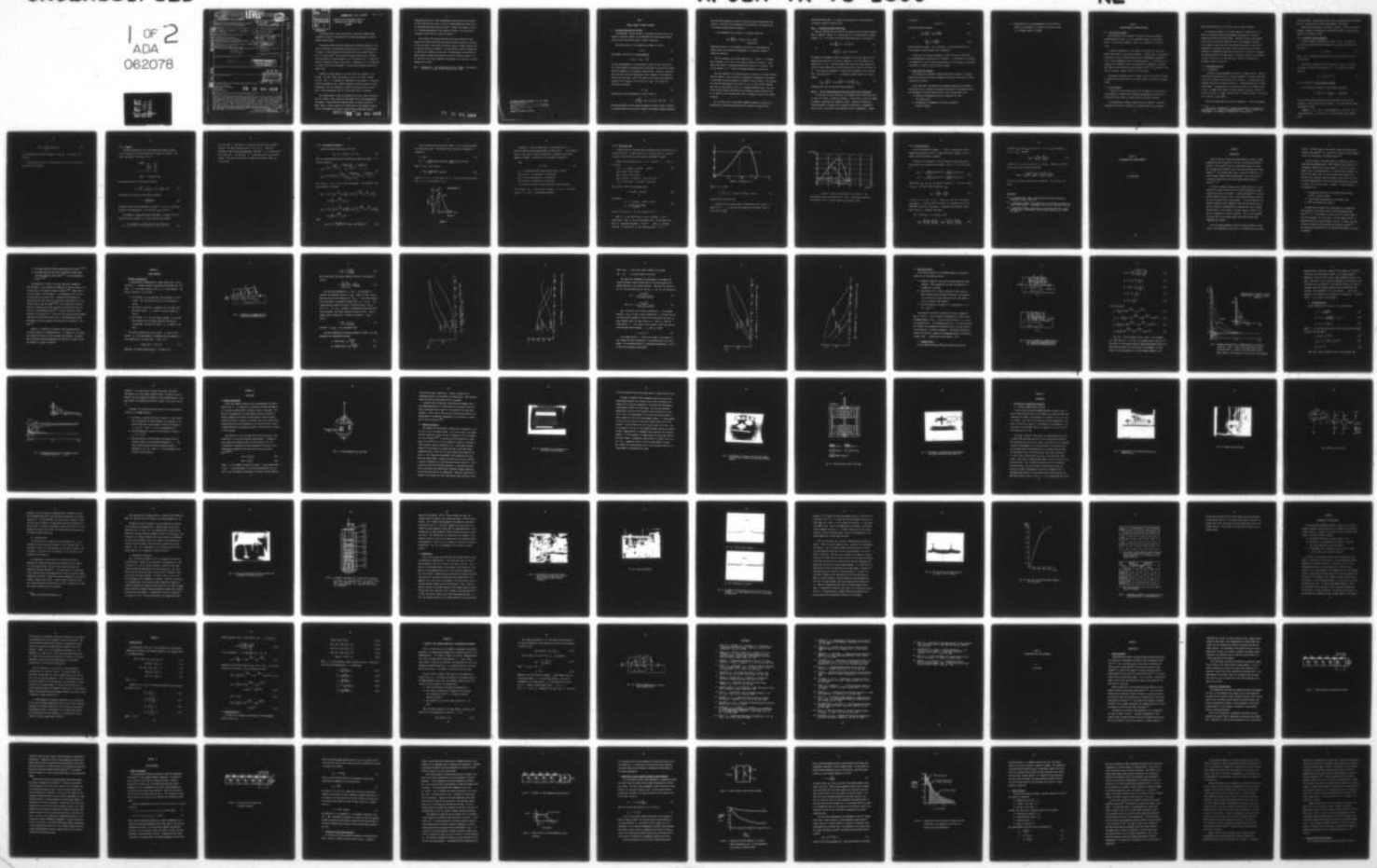

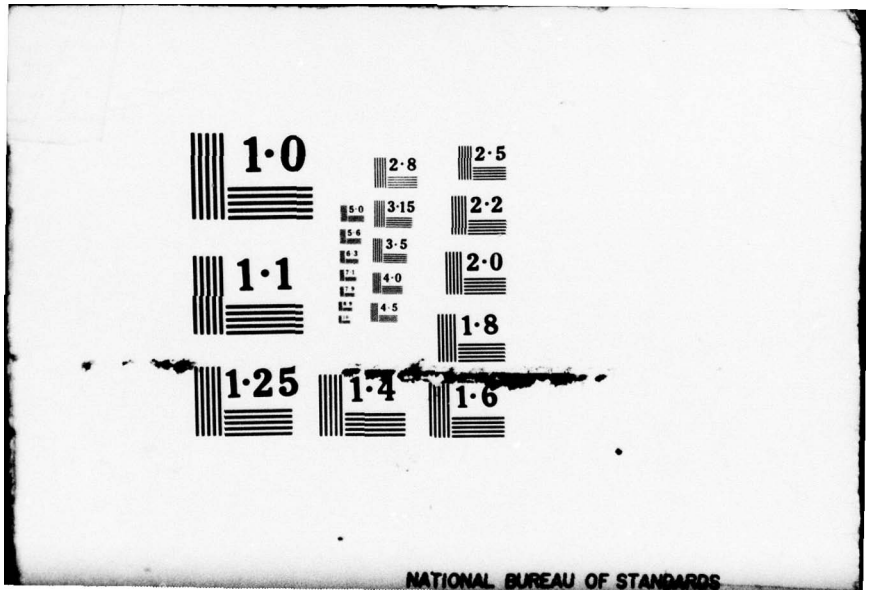
1·0
1·1
1·25
1·4
1·6
1·8
2·0
2·2
2·5
2·8
3·15
3·5
4·0
4·5
5·0
5·6
NATIONAL BUREAU OF STANDARDS

UNCLASSIFIED
SECURITY CLASSIFICATION OF THIS PAGE (When Data Entered)

LEVEL II

REPORT DOCUMENTATION PAGE

READ INSTRUCTIONS BEFORE COMPLETING FORM

1. REPORT NUMBER	2. GOVT ACCESSION NO.	3. RECIPIENT'S CATALOG NUMBER
AFOSR-TR-78-1500		

4. TITLE (and Subtitle)
THEORETICAL AND EXPERIMENTAL STUDY OF SUPER-CONDUCTING INDUCTIVE STORAGE SYSTEMS.

5. TYPE OF REPORT & PERIOD COVERED
Final Report.
August 1976 - July 1978

6. PERFORMING ORG. REPORT NUMBER

7. AUTHOR(s)
O. K. Mawardi, D. Hazony, H. K. Chung, & Leo D. Holland

8. CONTRACT OR GRANT NUMBER(s)
AFOSR-76-2886

9. PERFORMING ORGANIZATION NAME AND ADDRESS
Plasma Research Laboratory
Case Western Reserve University
University Circle, Cleveland, Ohio 44106

10. PROGRAM ELEMENT, PROJECT, TASK AREA & WORK UNIT NUMBERS
2301/A7
61102F
A7

11. CONTROLLING OFFICE NAME AND ADDRESS
Airforce Office of Scientific Research (AFSC)
Directorate of Physics (NP)
Bolling Air Force Base, D.C. 20332

12. REPORT DATE
October 17, 1978

13. NUMBER OF PAGES
126 pages

14. MONITORING AGENCY NAME & ADDRESS (if different from Controlling Office)
122p.

15. SECURITY CLASS. (of this report)
Unclassified

15a. DECLASSIFICATION/DOWNGRADING SCHEDULE

16. DISTRIBUTION STATEMENT (of this Report)
Approved for public release; distribution unlimited.

DISTRIBUTION STATEMENT A
Approved for public release;
Distribution Unlimited

17. DISTRIBUTION STATEMENT (of the abstract entered in Block 20, if different from Report)

DDC RECEIVED DEC 11 1978 D

18. SUPPLEMENTARY NOTES

19. KEY WORDS (Continue on reverse side if necessary and identify by block number)
Inductive Storage
Pulse Inductive Storage
Flux Pumps
Shaping Circuits

78 12 04.046

20. ABSTRACT (Continue on reverse side if necessary and identify by block number)
This report covers a two year effort to develop efficient pulse inductive storage sources. Two schemes have been considered in details. One scheme is based on the electromagnetic dual of the classic Marx generator. In the other scheme a pulse shaping circuit has been used to improve the energy transfer from the storage to the load. In the process of these investigations two types of flux pumps have been investigated. These superconducting devices are ideal to provide the charging current to the inductors. Fast acting pumps were designed and built. Their response is several orders of magnitude better than is currently available.

DD FORM 1 JAN 73 1473 EDITION OF 1 NOV 65 IS OBSOLETE

UNCLASSIFIED 416969 LB
SECURITY CLASSIFICATION OF THIS PAGE (When Data Entered)

AD A062078

DDC FILE COPY

AFOSR-TR- 78-1500

OCT 2 0 1978

THEORETICAL AND EXPERIMENTAL STUDY OF SUPERCONDUCTING INDUCTIVE STORAGE SYSTEMS

Introduction

The present report covers work performed under Grant AFOSR-76-2886 concerning a series of investigations on pulsed superconducting inductive energy storage systems.

The general purpose of these studies was to establish guidelines to be used in the design of pulsed energy sources repetitive or for single bursts of energy. In most applications encountered the load is highly inductive. Now, it is well known[1] that capacitive storage systems are not economic once the energy to be stored exceeds the 100 kilojoules level. A capacitive system is inherently a high voltage system. Consequently, all its components are costly since they are designed to operate under sustained conditions of high voltage.

Inductive storage systems, on the other hand, are "charged" at low voltage. The high voltage does appear, but only at the time of energy delivery. Then, it is comparable in magnitude to the voltage of a capacitive system of appropriate size. Another advantage of inductive system is their compactness. The cost estimated in terms of dollars per joule as stated above is more advantageous once the 100 kilojoule level is exceeded.

The disadvantages of inductive systems are the ohmic losses associated with the storage. These losses are high enough that it has instigated the development of superconducting inductors which, of course, are free of ohmic losses. In many instances, the added cost of the cryogenic installation is out-weighed by the overall economic gain obtained when using a

superconducting system. Other disadvantages associated with such systems are the relatively poor state of the art of superconducting switches and of superconducting power supplies needed to "charge" the inductors. Finally, a serious disadvantage of the inductive storage is its inefficiency in energy transfer when the "load" is inductive.

In the series of investigations which have been performed at CWRU, several of the objections encountered above have been successfully resolved. In the first part of this report the general theory of energy transfer from an inductive system is discussed. In the second part, specific suggestions of improving the transfer are outlined. The experimental verifications of these concepts by Chung and Holland are included in parts III and IV. In the last part of the report suggested improvements in the design of inductive systems are described.

Ref. 1 - Carruthers, R., "The Storage and Transfer of Energy", High Magnetic Fields, ed. by Kolm, The MIT Press, pp. 307, 1962.

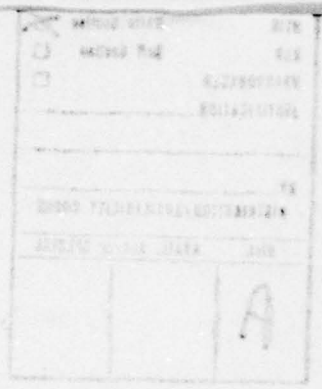

AIR FORCE OFFICE OF SCIENTIFIC RESEARCH (AFSC)
NOTICE OF TRANSMITTAL TO DDC
This technical report has been reviewed and is
approved for public release IAW AFR 190-12 (7b).
Distribution is unlimited.
A. D. BLOSE
Technical Information Officer

PART I

GENERAL THEORY OF ENERGY TRANSFER

I.1 Governing Relations for Transfer

The mechanism of energy transfer of the magnetic energy stored in an inductor to another inductor can be described in the most general manner and from first principles by means of Maxwell equations.

The starting point of the arguments are Ampère's relation

$$\nabla \times \underline{H} = \underline{J} \tag{1}$$

and Faraday's relation for a moving conductor

$$\nabla \times (\underline{E} + \underline{v} \times \underline{B}) = - \frac{\partial \underline{B}}{\partial t} \tag{2}$$

The term corresponding to the displacement current has been omitted from (1) for the purpose of de-emphasizing the importance of the electric energy stored by comparison to the magnetic energy stored. Stated in a different way we can state that the displacement current compared to the conduction current is of the order $(v/c)^2$, the square of the ratio of the mechanical velocity of the conductor to the velocity of light. By invoking the constitutive relations

$$\underline{B} = \mu_o \underline{H} \tag{3}$$

manipulation of the two equations (1) and (2) leads to

$$\frac{\partial}{\partial t} \left(\frac{B^2}{2\mu_o}\right) = \underline{E} \cdot \underline{J} + \underline{v} \cdot \underline{J} \times \underline{B} + \nabla \cdot (\underline{E} \times \underline{H}) \tag{4}$$

The above expression is well known and appears in several classic textbooks. It actually states that the rate of change of the magnetic energy associated

with the moving conductor is equal to the electric power supplied from the battery, to the rate of the mechanical work performed on the conductor and to the power radiated from the conductor.

If one integrates over all space, it is readily found that

$$\frac{\partial}{\partial t}\int \left(\frac{B^2}{2\mu_o}\right)d\tau = \int \underline{E}\cdot\underline{J}d\tau + \int(\underline{v}\cdot\underline{J} \times \underline{B})d\tau + \int(\underline{E} \times \underline{H})\cdot d\underline{\sigma} \qquad (5)$$

The above equation (5) is now applied to the case of a superconducting inductor and to the situation corresponding to an impulsive transfer of energy from inductors.

The first integral on the right hand size viz., $\int \underline{E}\cdot\underline{J}d\tau = 0$ everywhere. This is because $\underline{J} \neq 0$ only in the volume enclosing the conductor. Consequently the volume of integration becomes the volume of the conductor. But in the conductor $E = 0$, hence the integral vanishes as stated above.

The last integral on the right hand side is related to the energy radiated from the inductor. Now the surface of integration corresponds to the surface of the conductor plus the surface of a sphere of infinite extent. The contribution from the large sphere is zero since $E \sim \frac{1}{r}$, $H \sim \frac{1}{r^2}$ and the integrand goes like $\frac{1}{r}$ which tends to zero as r becomes infinitely large. The value of the surface integral evaluated over the conductor usually vanishes since $E = 0$ except for the time when the circuit is opened to initiate the transfer of energy.

Eq. (5) turns out to a very useful expression because it allows one to discuss most of the cases associated with the transfer of energy from a

superconducting inductor. To illustrate the generality of this expression we consider a number of typical cases.

Case I No Mechanical Motion Takes Place

When the conductor does not move one is dealing with the classic situation where a "charged" inductor L_1 delivers part of its stored energy to another inductor L_2. It is clear for this particular case that Eq. (5) reduces to

$$\frac{\partial}{\partial t}\left(\int \frac{B^2}{2\mu_o}\, d\tau\right) = \int (\underline{E} \times \underline{H})\cdot d\sigma \tag{6}$$

or

$$\int \frac{B^2}{2\mu_o}\, d\tau \Big|_0^{\infty} = \int_0 dt \int (\underline{E} \times \underline{H})\cdot d\sigma \tag{7}$$

The change in the magnetic energy is thus equal to the total energy that has escaped from the system in the form of radiation. To fix the ideas let us assume that $L_1 = L_2$. This then implies that after the energy transfer the current in each inductor will be one half the initial value of the current in L_1. From similarity arguments it follows that the magnetic field is halved also. This means that at $t = \infty$, the magnetic energy stored in the system becomes:

$$\int_{\text{coil 1}} \frac{B^2}{2\mu_o}\, d + \int_{\text{coil 2}} \frac{B^2}{2\mu_o}\, d\tau = 2\left(\frac{1}{4}\int \frac{B^2}{2\mu_o}\, d\tau \Big|_{t=0}\right) \tag{8}$$

indicating that half the energy has been dissipated.

Case II The Coil Moves Impulsively, But the Circuit is Not Interrupted

In this case, the last term of Eq. (5) vanishes since the Poynting vector is zero at all times. An important property of this circuit is that the change of magnetic energy goes into mechanical energy. Because the system has become reversible it behaves like an adiabatic system from a thermodynamic point of view. The proof of this assertion is easy to demonstrate. Indeed

if we write

$$\underline{J} \times \underline{B} = m\, \dot{v} \tag{9}$$

The modified equation becomes

$$\frac{\partial}{\partial t} \int \frac{B^2}{2\mu_o} d\tau = \frac{\partial}{\partial t} \int (\frac{m v^2}{2}) d\tau \tag{10}$$

or

$$\frac{B^2}{2\mu_o} d\tau = \int (\frac{m v^2}{2}) d\tau \tag{10}'$$

which completes the proof. It is clear that $\underline{v}$ could stand equally well for an angular velocity without loss of generality.

A corollary to the above conclusions is that from the well known work on electromechanical analogies one can visualize v as equivalent to the charge on a capacitor so that the results obtained above are that energy is transferred from kinetic to potential form without any losses.

I.2 Basic Rules for Transfer

The transfer of the magnetic energy stored from an inductor to a purely resistive load does not pose any fundamental difficulties since all the energy stored can be utilized.

On the other hand, the transfer of the magnetic energy from one inductor into another can be a dissipative process as was shown in the previous section. The discussion of the same section points to the following basic rules

1) Inductors discharging directly into inductors will lead to an energy loss.
2) The addition of condensers to the circuit makes the transfer lossless.

3) The provision of an electromechanical converter which is known to be equivalent to a capacitive system also leads to a lossless transfer of energy.

PART II

IMPROVED METHOD OF ENERGY TRANSFER

II.1 Pure Inductive System

The efficiency for the transfer of energy for the purely inductive system discussed in Case 1 of I.1 is obviously related to a geometrical factor. An equivalent statement is that it is a function of the ratio of L_1/L_2.

To study the generality of this effect one considers the case of the energy being stored in more than one inductor. Actually when a series/parallel combination is used it becomes apparent that an advantageous arrangement is that of the electromagnetic dual of the Marx generator. In this scheme, the inductors are "charged" in series and subsequently "discharged" in parallel. The theory for this scheme was first reported in 1977.[2] The details of the proof is covered at length in Part III of this report.

The essential conclusion that is reached is that the transfer efficiency is improved from the 25% value for two equal inductor to 33% with the present scheme.

II.2 The L-C System

It was seen in the previous section that the addition to the system of another degree of freedom (either through electromechanical conversion or through capacitors) makes the system reversible and hence lossless.

The disadvantage in adding a capacitive system, however, is that the condensers must be able to handle all the energy stored in the inductors.

Under these conditions the cost of the system is unduly increased.

An alternative approach to the simple addition of capacitance to the system is to examine various pulse shaping circuits made up of lossless components (inductors and capacitances). Although the use of pulse shaping circuits does not alter the condition that all the condensers eventually have to handle a major fraction of the energy stored there is the definite improvement of preventing the current from oscillating (hence no current reversal) and consequently improving the efficiency of transfer by minimizing the mismatch between the storage system. The general theory of pulse shaping is given in Section II.3 of this part while a specific configuration is discussed in details in Part IV.

II.3 Pulse-Shaping Circuit*

II.3.1 Introduction

Of concern is pulse management and control in dynamic systems. Normally, unless special conditions are met, the pulse response of a dynamic system shall have tails or asymptotes that stretch out to infinity. A transducer may keep vibrating long after the original excitation. An antenna may stretch the transmitted signal. A stepping motor may continue to vibrate for extended periods of time. A communication channel may cause signals to overlap. Similarly, a filter in the path of a signal, may serve well to scrub the signal off its noise, but a long tail is also added.

Gerst and Diamond posed this problem in Reference 3. They also suggested

---

*This section contributed by D. Hazony was presented at a Conference in honor of Prof. R. J. Duffin at Carnegie-Mellon Univ., July 10-14,1978. The proceedings of the conference will appear soon in a book form.

several solutions. Philipp Dines and the author continued the work and showed that it is also possible to control some aspects of the output.

These works are reviewed in this paper. Moreover, it will be seen that a number of degrees of freedom may be added which need be no larger than the degree of the network plus one.

II.3.2 The Finite Laplace Transform

Consider a dynamic system where the input is $e_i(t)$, the output is $e_o(t)$ and they have the Laplace Transforms E_1 and E_2 governed by the relationship

$$E_1 = t_{21} E_2 \tag{1}$$

where $t_{21}(s)$ represents the transfer function of an initially relaxed dynamic system.

The problem is reduced to that of obtaining an input e_i such that the output is confined to the interval $0,T$. This defines a Laplace transform:

$$E_2 = \int_0^T e_o(t)\, e^{-st}\, dt \tag{2}$$

which is denoted as a finite Laplace transform.

The following are examples of finite Laplace transforms:

$$\frac{(1 - \exp - s)}{s}\ ,\ \frac{1 - \exp - s}{s^2 + 1}\ ,\ \frac{1 - \exp - (s+1)}{s + 1} \tag{3}$$

Note that these functions have their poles cancelled by zeros of the numerators. Hence they are entire functions. It has been proved by Gerst and Diamond [1] that:

Theorem 1: If P_i and D are polynomials in s with the P_i's of lower degree than D, and if the a_i's are non negative real numbers, then:

$$G(s) = \frac{1}{D} \sum_{i=1}^{k} P_i \exp(-a_i s) \qquad (4)$$

is a finite Laplace transform of length $a(= \max a_i)$ if, and only if, it is entire.

In what follows we shall insist that both E_1 and E_2 shall satisfy the conditions of Theorem 1.

II.3.3 Examples

The basic procedure will be illustrated by the following example. It will also serve to bring out some special features of interest. Consider the Low-Pass filter shown in Fig. 1.

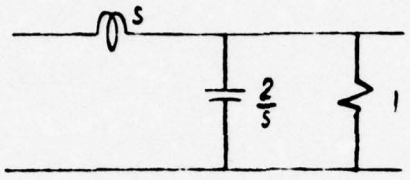

Figure 1. Low Pass Filter

The voltage transfer function of this filter is:

$$t_{21} = \frac{E_2}{E_1} = \frac{2}{s^2 + 2s + 2} = \frac{2}{(s + 1 + j)(s + 1 - j)} \tag{5}$$

One possible input would have the Laplace transform:

$$\frac{1 - \exp(-as-a)}{s + 1} \tag{6}$$

provided of course that the numerator is zero at $(s + 1 \pm j) = 0$ which are the zeros of the denominator. This restricts a_{min} to be 2π .

This example is suggested by Gerst and Diamond. To remove this last restriction on the interval 'a' they suggested the following:

$$E_1 = \frac{(1 - \exp - \frac{a}{3} s)(1 - \exp - \frac{a}{3} (s+1+j))(1 - \exp - \frac{a}{3} (s+1-j))}{s} \tag{7}$$

The first term $(1 - \exp -\frac{a}{3} s)/s$ is inserted to make the input piecewise constant. The other terms are zero at $(s + 1 \pm j) = 0$. Gerst and Diamond call their method zero insertion. Note that 'a' is arbitrary and can be very small. The fact that 'a' is arbitrary permits optimization schemes. These can be carried out in respect to efficiency, shape, or output energy.

II.3.4 Development for Degree 2

Applying the above technique to the filter:

$$t_{21} = (\alpha^2 + \beta^2)/[(s + \alpha)^2 + \beta^2] \quad , \tag{8}$$

Gerst and Diamond determined the following input-output pair where T is the pulse duration;

$$E_i(s) = \frac{\left(1 - e^{-\frac{Ts}{3}}\right)\left(1 - e^{-\frac{T(s+\alpha-j\beta)}{3}}\right)\left(1 - e^{-\frac{T(s+\alpha+j\beta)}{3}}\right)}{s} \quad ,$$

$$E_o(s) = \frac{(\alpha^2 + \beta^2)\left(1 - e^{-\frac{Ts}{3}}\right)\left(1 - e^{-\frac{T(s+\alpha-j\beta)}{3}}\right)\left(1 - e^{-\frac{T(s+\alpha+j\beta)}{3}}\right)}{s[(s+\alpha)^2 + \beta^2]} \quad . \tag{9}$$

Let $u(t-t_o) = 1$ for $(t \geq t_o)$ and zero elsewhere. The following is the time response of the above

$$e_i(t) = u(t) - \left(1 + 2e^{-\frac{T\alpha}{3}} \cos\frac{T\beta}{3}\right) u(t - \tfrac{T}{3}) + \left(e^{-\frac{2T\alpha}{3}} + 2e^{-\frac{T\alpha}{3}} \cos\frac{T\beta}{3}\right)$$
$$u(t - \tfrac{2T}{3}) - e^{-\frac{2T\alpha}{3}} u(t-T) \quad ,$$

$$e_o(t) = r(t) - \left(1 + 2e^{-\frac{T\alpha}{3}} \cos\frac{T\beta}{3}\right) r(t - \tfrac{T}{3}) + \left(e^{-\frac{2T\alpha}{3}} + 2e^{-\frac{T\alpha}{3}} \cos\frac{T\beta}{3}\right) *$$
$$r(t - \tfrac{2T}{3}) - e^{-\frac{2T\alpha}{3}} r(t-T) \quad ,$$

where

$$r(t) = \left(1 - \frac{(\alpha^2 + \beta^2)^{\frac{1}{2}}}{\beta} e^{-\alpha t} \cos(\beta t - \tan^{-1}\tfrac{\alpha}{\beta})\right) u(t) \quad . \tag{10}$$

Thus the method has one arbitrary constant. It is piecewise constant with three equal steps. The following input function was suggested in Reference 4.

$$E_1 = N_1/s \tag{11}$$

$$N_1 = 1 - \frac{\sin b}{\sin(b-a)} \exp(-a(s+\alpha)/\beta) + \frac{\sin a}{\sin(b-a)} \exp(-b(s+\alpha)/\beta)$$

where a and b are roots of:

$$f = \frac{\cos x - \exp(-x\alpha/\beta)}{\sin x} = \text{constant} \tag{12}$$

Setting $s = 0$, or $-\alpha \pm j\beta$ gives $N_1 = 0$. A typical input-output plots (for $\alpha = \beta = 1$) are shown in Fig. 2.

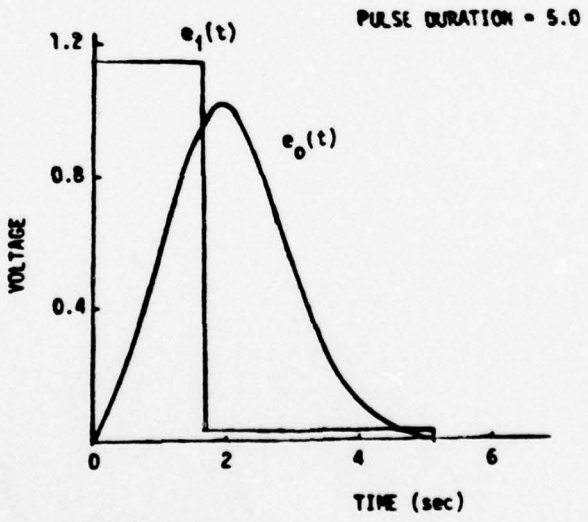

Figure 2

A study of f (Eq. 12) shows that it is multivalued for $x > \pi$. Hence the resulting minimum pulse length is larger than π. The following function (N_1 in Eq. 13) has no length limit. Moreover it has three degrees of freedom. The function will be derived in Section 6.

Thus:

$$E_1 = N_1/s \tag{13}$$

$$N_1 = 1 + A \exp(-a(s+\alpha)/\beta) + B \exp(-b(s+\alpha)/\beta) + C \exp(-c(s+\alpha)/\beta)$$

$$AD = \sin(a-c) + \sin c \exp -b\alpha/\beta - \sin b \exp -c\alpha/\beta$$

$$BD = \sin(c-a) + \sin a \exp -c\alpha/\beta - \sin c \exp -a\alpha/\beta$$

$$CD = \sin(a-b) + \sin b \exp -a\alpha/\beta - \sin a \exp -b\alpha/\beta$$

$$D = \sin(a-c) \exp -b\alpha/\beta + \sin(c-b) \exp -a\alpha/\beta + \sin(b-a) \exp -c\alpha/\beta$$

This function (N_1) is zero at the origin and $s = -\alpha \pm j\beta$. The break points, a, b, and c, are perfectly arbitrary.

II.3.5 The Bipolar Case

A bipolar pulse is relatively easy to produce either by switching or by hard amplification. In what follows it will be shown that it is possible to obtain a time limiting bipolar pulse for the degree 2 network.

Without loss in generality let $\alpha = \beta = 1$ and let $c = \pi$ in Eq. 13. This gives

$$N_1 = 1 - c_1 \exp{-as} + c_2 \exp{-bs} - c_3 \exp{-\pi s} \tag{14}$$

$$C_4 C_1 = \sin b(1 + \exp{-\pi}) \exp{-a}$$

$$C_4 C_2 = \sin a(1 + \exp{-\pi}) \exp{-b}$$

$$C_4 C_3 = (\sin(a-b) + \sin b \exp{-a} - \sin a \exp{-b}) \exp{-\pi}$$

$$C_4 = \sin(b-a) \exp{-\pi} + \sin b \exp{-a} - \sin a \exp{-b}$$

This function simplifies considerably when

$$\sin a \exp a = \sin b \exp b = K \tag{15}$$

Accordingly:

$$N_1 = 1 - C_1(\exp{-as} - \exp{-bs}) - \exp{-\pi s}$$

$$C_1 = \frac{\sin b(1 + \exp\pi) \exp{-a}}{\sin(b-a)} \tag{16}$$

A plot of $\sin x \exp x$ vs x (Eq. 15) is shown in Fig. 3.

When $K \to 0$ the coefficients a and b approach 0 and π respectively. Then C_1 (Eq. 16) approaches unity. On the other hand when $b-a$ approaches zero (near $x = 3\pi/4$) makes C_1 approach infinity. It follows that C_1 may assume any value $1 < C_1 < \infty$.

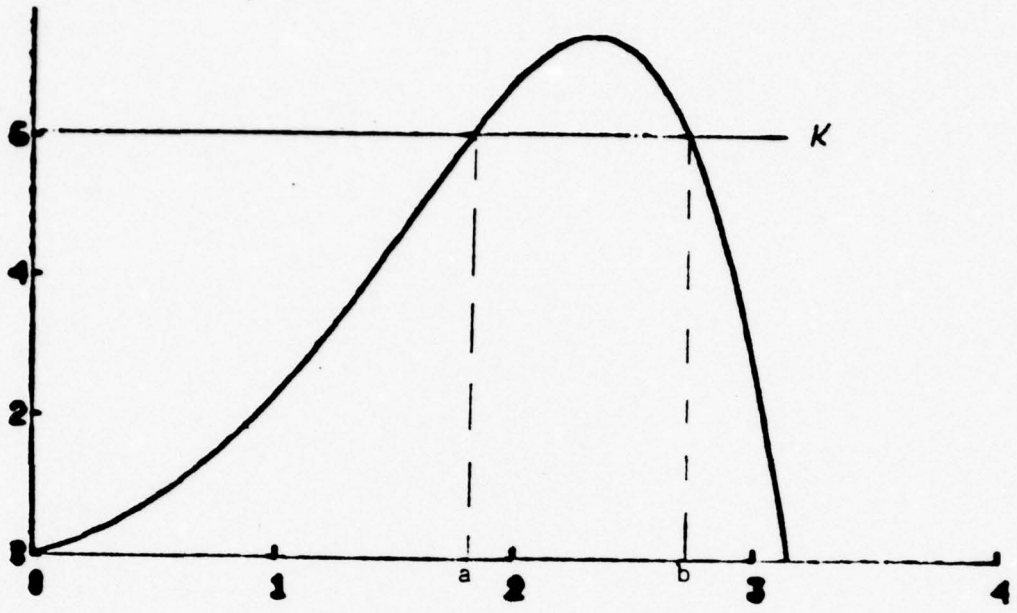

Figure 3. sinx expx vs. x

Making $C_1 = 2$ gives:

$$E_1 = \frac{N_1}{s} = \frac{1}{s}\,(1 - 2\,\exp{-as} + 2\,\exp{-bs} - \exp{-\pi s}) \qquad (17)$$

representing the bipolar pulse.

A computer plot of output signals corresponding to Eqs. 9 and 17 is shown in Fig. 4. It is seen that the response to the bipolar input is significantly higher.

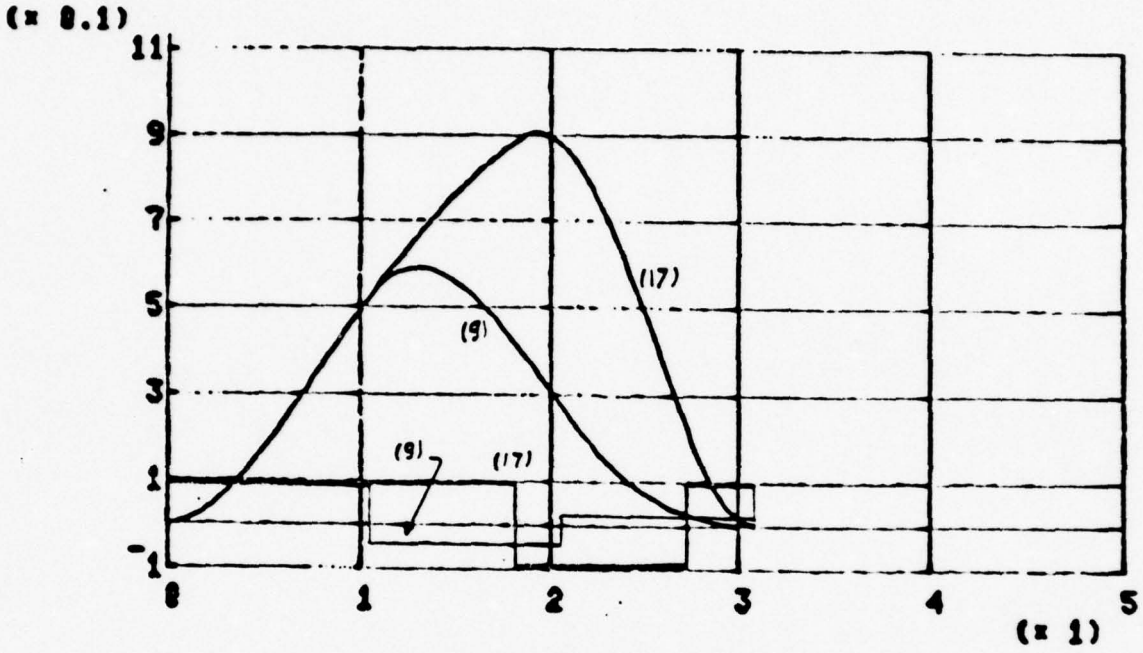

Figure 4. Outputs Corresponding to Eqs. 9 and 17. The corresponding inputs are shown with 10:1 scale. The energy delivered to the resistor (Fig. 1) is about double for the bipolar input.

II.3.6 The Main Theorem

Given an RLC network of degree n. Then it is possible to find a stepwise constant pulse, with $n+1$ steps of arbitrary lengths, which will evoke a time limited network response.

The proof is an induction. It will be shown that new poles can be cancelled by the introduction of new steps. Let N_1 in Eq. 11 be written as:

$$F_{ab} = 1 - \frac{\sin b}{\sin(b-a)} \exp -a(s+\alpha)/\beta + \frac{\sin a}{\sin(b-a)} \exp -b(s+\alpha)/\beta$$
$$F_{bc} = 1 - \frac{\sin c}{\sin(c-b)} \exp -b(s+\alpha)/\beta + \frac{\sin b}{\sin(c-b)} \exp -c(s+\alpha)/\beta \qquad (18)$$

Clearly both F_{ab} and F_{bc} are zero at $(s+\alpha \pm j\beta) = 0$. Let $F(0)$ denote $F(s)\big|_{s=0}$. Then the following function, F_{abc},

$$F_{abc} = \frac{F_{ab}}{F_{ab}(0)} - \frac{F_{bc}}{F_{bc}(0)} \qquad (19)$$

is zero at $s = 0$, and $-\alpha \pm j\beta$. In fact N_1 (Eq. 14) is the same as $F_{abc}/F_{abc}(\infty)$. It follows that this process will generate a zero for any additional real pole of the network. To generate an additional complex pole, say at s_o, proceed in two steps:

Let $U = \text{Re } F(s_o)$, $V = \text{Im } F(s_o)$, and

$$G_{abc} = \frac{U_{bc} F_{ab} - U_{ab} F_{bc}}{U_{bc} V_{ab} - U_{ab} V_{bc}}, \quad G_{bcd} = \frac{U_{cd} F_{bc} - U_{bc} F_{cd}}{U_{cd} V_{bc} - U_{bc} V_{cd}} \qquad (20)$$

Thus both G_{abc} and G_{bcd} are zero at $s = -\alpha \pm j\beta$ and are equal to j at $s = s_o$. Therefore

$$F_{abcd} = \frac{G_{abc} - G_{bcd}}{G_{abc}(\infty) - G_{bcd}(\infty)} \tag{21}$$

is zero at $s = -\alpha \pm j\beta$ as well as s_o, and $\bar{s}_o$. Moreover to produce a zero at the origin we add one more point:

$$F_{abcde} = \frac{F_{bcde}(0)\, F_{abcd} - F_{abcd}(0)\, F_{bcde}}{F_{bcde}(0)\, F_{abcd}(\infty) - F_{abcd}(0)\, F_{bcde}(\infty)}$$

Similarly, any number of zeros would be generated. This completes the proof.

References

2) O. K. Mawardi and H. Chung, Proceedings International Pulsed Power Conference, Lubbock, Texas 1976.

3) I. Gerst and J. Diamond, "The Elimination of Intersymbol Interference by Input Signal Shaping," Proceedings of the IRE, pp. 1195-1203, July 1961.

4) P. Dines and D. Hazony, "Optimization of Time Limited Outputs in Band Limited Channel", Proceeding of 13th Allerton Conference, pp. 515-522, Oct. 1975.

PART III

A SUPERCONDUCTING SKRAM GENERATOR

by

HO KYOON CHUNG

CHAPTER I

INTRODUCTION

Since the advent of high field superconductors, inductive energy storage has become attractive not only as a load levelling method in electric utility system[1] but as a pulsed power source for lasers and electron beam sources[2], and for controlled theormonuclear fusion reactors.[3] As a pulsed power source, it has been shown that an inductive energy storage system has advantages in size and cost over a capacitive storage when the stored energy exceeds around 10^5 joules.[4], [5]

In order to transfer energy from the storage inductor to a load, there has to be some interface circuit, which determines the energy transfer efficiency of the system. A survey by Komarek[6] illustrates several possible transfer circuits, their maximum efficiency obtainable, and the design limits of each scheme. It is well known that the simplest transfer circuit composed of shunt and series switches only has an efficiency of maximum 25% for a matched load, and to upgrade the efficiency it is necessary to include a reactive element in the form of a capacitor or a mutual inductance. This in turn increases the total cost of the storage system, since equally high rating components are required.

One of the major problems in inductive energy storage is encountered in the technological limitation of the switches for the transfer

circuits. Different types of the current breakers have been used at different time scales[7], and a great deal of effort is being expended to meet the requirements for each application.[8]

The main concern of this work has been a feasibility study on a superconducting SKRAM generator, which produces a high current out of the magnetic energy stored in many inductors. This is an electromagnetic dual of the Marx generator, in the sense that a number of inductors are charged first in a series connection and then all are switched into a parallel circuit to produce a high current in a load. (The name SKRAM generator is derived from Marx generator by reversing the order of the letters of Marx (or Marks). The main features of this generator are:

1) An improved efficiency over the simple transfer scheme without a reactive element.
2) Less stringent requirements on the switches, and
3) Shorter discharge time constant.

Although several methods have been worked out to minimize the heat loss due to feed current leads to the superconducting magnets,[9], [10] it is preferable to avoid the use of current leads to the liquid He dewar if it can be done. For this reason, current is generated within the liquid He bath by a device, so called, flux pump, on which an extensive review was done by the group at Leiden.[11] Flux pumps can be classified into two categories according to the mode of operation.

1) Flux pumps employing discrete superconducting switches.[12-15]
2) Flux pumps employing flux spots transported through superconducting sheets by light beams[16], or by moving magnetic fields.[17-21]

The generation of current flux pumps invariably accompanies heat dissipation, and a qualitative comparison on the efficiency of the various types of flux pumps was made by Newhouse.[22] Among those in the last category, the flux pump of a rotating-magnet type is one of the most popular and widely used. Although several mathematical formulations have been made on the operational characteristics of the similar types of the flux pumps[23-25], and an appreciable amount of empirical informations has been obtained on the emf due to the flux motion in a superconducting sheet[26], an exact theoretical understanding is not achieved yet. There still exist many unsolved problems associated with the moving normal spot in the superconducting sheet and rather an intuitive approach has been used in the design of flux pump.[27]

Chapter II is devoted to the general considerations and the transient analysis of the SKRAM generator. In Chapter III, the design and construction details of the flux pump are discussed. The experimental apparatus and the measurements are described in Chapter IV and the summary is included in Chapter V.

CHAPTER II

SKRAM GENERATOR

1. General Considerations

A superconducting SKRAM generator, shown schematically in Fig. 1 , consists of n storage inductors, superconducting switches and a flux pump. L_1's are storage inductors, and L_2 is a load inductor. The method of operation is as follows.

1) The switches S_1's are kept open, while switches S's are closed. This interconnections put all the inductors in series.
2) The series of inductors is charged by the flux pump, and a persistent current I_i is made to circulate around the circuit.
3) The switches S_1's are now closed, and <u>then</u> S's are open. This converts all the storage inductors into parallel configuration, and the final current I_f is induced in the load.

The relation between the initial current I_i and the final current I_f in the load inductor is obtained from the condition of flux conservation in the main loop ℓ (Fig. 1) as

$$I_f(L_2 + L_1/n) = I_i(L_1 + L_2) \qquad (1)$$

Therefore, the current amplification A is found to be

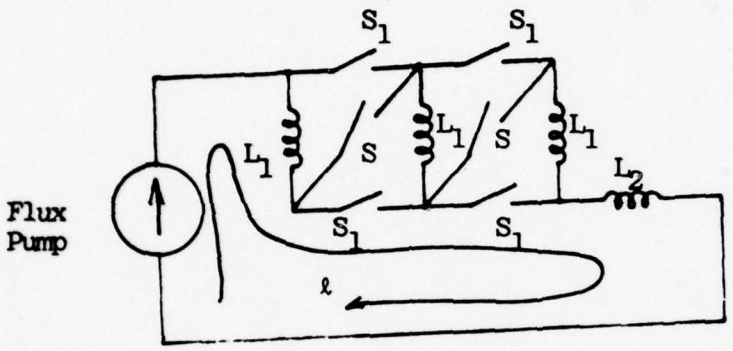

Fig. 1 A Schematic Representation of a Superconducting SKRAM Generator.

$$A = \frac{I_f}{I_i} = \frac{1 + L_1/L_2}{1 + L_1/nL_2} \tag{2}$$

On the other hand, the energy transfer efficiency of the system is given by

$$\eta = \frac{(I_f^2 - I_i^2)L_2}{I_i^2(L_2 + nL_1)} = \frac{A^2 - 1}{1+nL_1/L_2} \tag{3}$$

The functional dependence of A and η on the number of inductors for different values of L_1/L_2 is shown in Figs. 2 and 3. When many inductors are employed and $L_1/L_2 > 1$, the current amplification approaches its maximum attainable value $A_\infty = 1+L_1/L_2$. The highest maximum transfer efficiency of 33% occurs when $L_1/L_2 = 3$, and $n = 5$. As L_1/L_2 increases, the maximum efficiency drops and finally reaches to the lowest maximum efficiency of 25%. This is readily seen by reducing Eq. (3) under the condition $L_1/L_2 \gg 1$. That is,

$$\eta \approx \frac{L_1}{nL_2} \frac{1}{(1+L_1/nL_2)^2} \tag{4}$$

and when $n = L_1/L_2$, η has a maximum of 25%.

To better understand the system performance in detail, two other parameters are introduced as follows.

1) Loss factor $f_L \equiv \frac{W_i - W_f}{W_i}$ (5)

2) Residue factor $f_R \equiv \frac{W_f - W_{\ell f}}{W_i}$, (6)

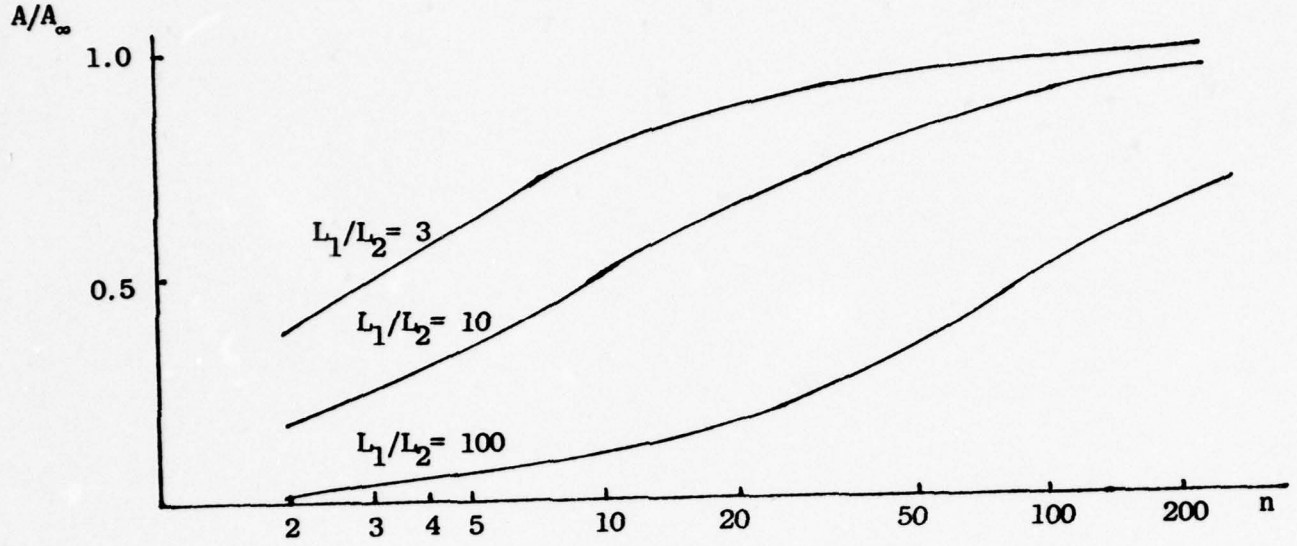

Fig. 2 Current Amplification vs. n for Different Values of L_1/L_2 , where $A_\infty = 1+L_1/L_2$.

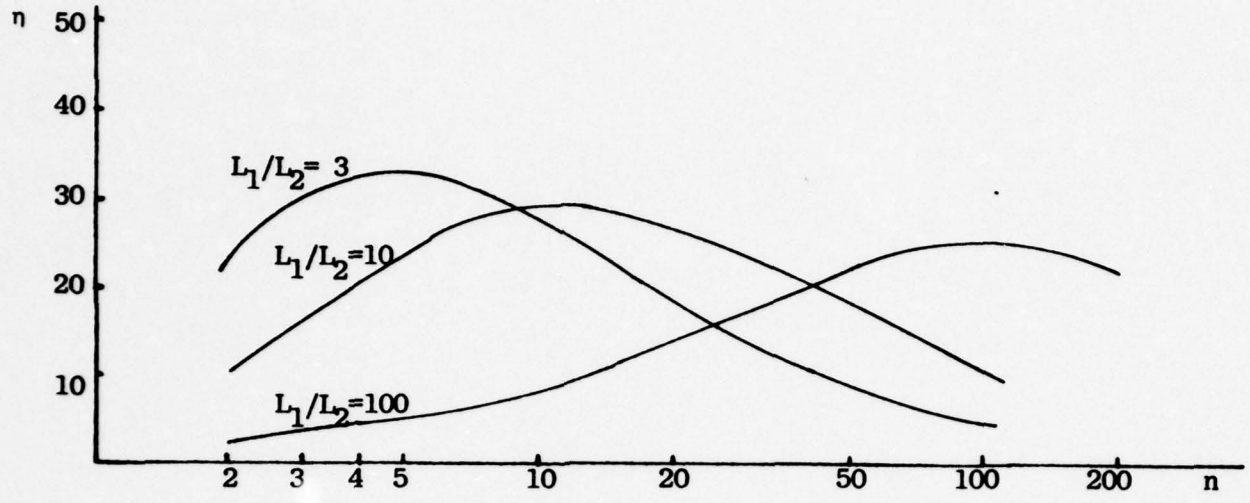

Fig. 3 Efficiency η vs. n for Different Values of L_1/L_2 .

where $W_{i(f)}$ = the initial (final) energy of the system

and $W_{\ell f}$ = the final energy in the load.

The loss factor determines the percentage of the energy loss during switching, and the residue factor is the percentage of the energy remaining in the storage inductors. Then from the relation of Eq. (1), and the definitions (5) and (6), f_L and f_R are obtained as

$$f_L = 1 - \frac{(1+L_1/L_2)^2}{(1+L_1/nL_2)(1+nL_1/L_2)} \tag{7}$$

$$\text{and } f_R = 1 - \frac{(1+L_1/L_2)^2}{(1+nL_1/L_2)(1+L_1/nL_2)^2} \tag{8}$$

Eqs. (7) and (8) are plotted as functions of n for different values of L_1/L_2 in Figs. 4 and 5, respectively. It is seen that the two factors have commutative effects on the efficiency such that f_R has a dominant effect for small value of n, while f_L does for large value of n. For a small initial current in the load inductor, the following relation between η, f_L and f_R holds.

$$\eta + f_L + f_R \tilde{\nu} 1 \tag{9}$$

For a large value of n, most of the energy of the system is lost through the power dissipation in the switches and is not recoverable. If the system returns to the charging configuration, $(1-f_L)^2$ of the initial energy is recoverable.

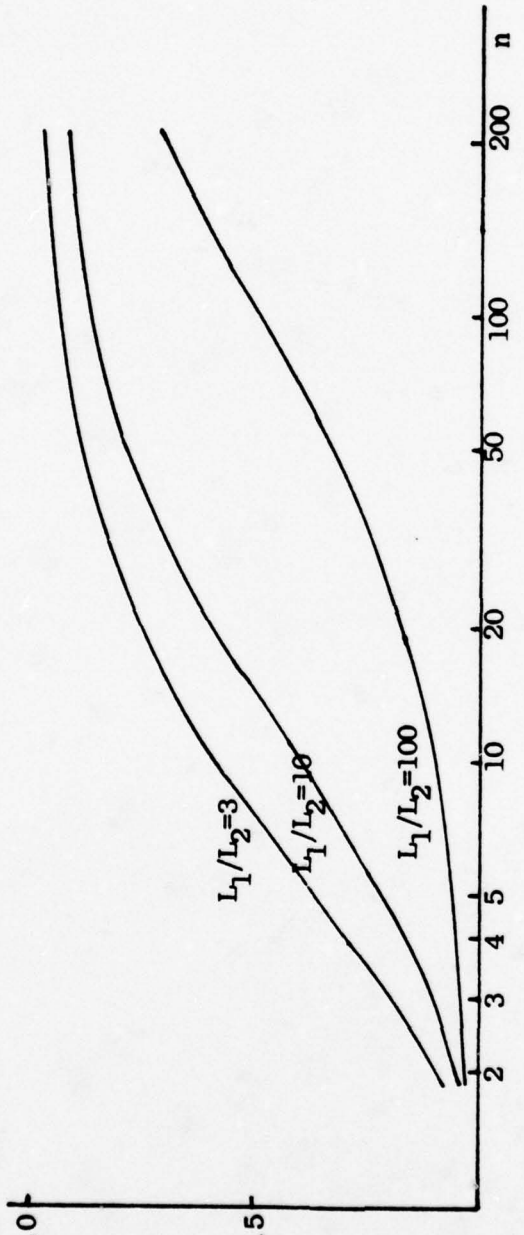

Fig. 4 Loss Factor f_L vs. n for Different Values of L_1/L_2 .

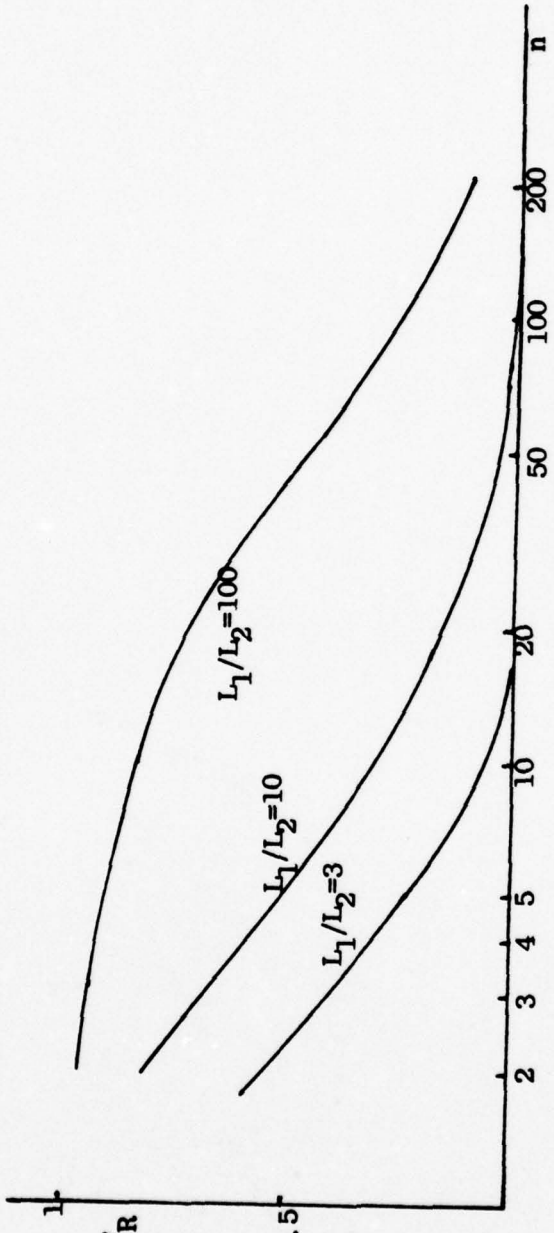

Fig. 5 Residue Factor f_R vs. n for Different Values of L_1/L_2

2. Transient Analysis

The transient condition of the SKRAM generator is analyzed in detail for the following conditions.

1) Pumping of magnetic flux into the storage inductors occurs stepwise. This is generally true when the generator is charged by a flux pump.
2) The switches have a finite resistance in open condition. When superconducting switches are employed, the resistance of the switches at normal state may not be high enough to allow the system a fast response.
3) For the simplicity of analysis, it is assumed that $n = 3$ and $L_1/L_2 = 3$.

The analysis is carried out based on the circuit diagrams of Fig. 6 (a) and (b). The flux pump is represented as a switch, which introduces magnetic flux Φ into the circuit at time $t = 0$ in (a), the charging period. In discharging period (b), it is short-circuited. The currents with alphabetical subscripts refer to the real currents in the inductors. As shown in Appendix I, the current through each inductor and switch in charging and discharging period is obtained as follows. Here τ stands for the time constant L_1/R .

A. Charging Period

In the complex frequency domain the currents are given by

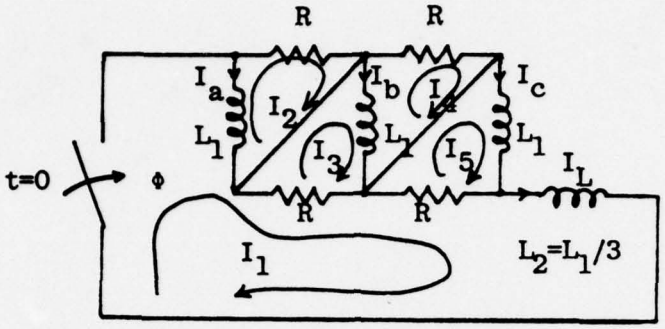

(a)

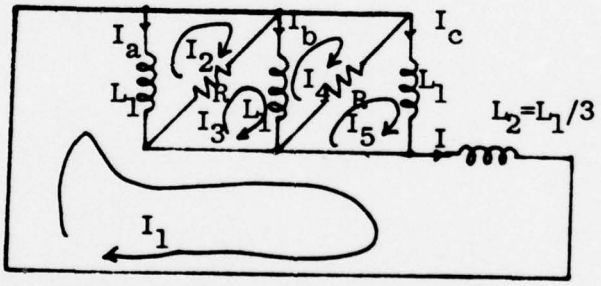

(b)

Fig. 6 Circuit Diagrams of a SKRAM Generator.
(a) During the Charging Period and
(b) During the Discharging Period.

$$I_L = I_1 = \frac{3\phi}{L_1} \frac{s^2 + \frac{3}{2\tau} s + \frac{1}{2\tau^2}}{s^2 + \frac{9}{\tau} s + \frac{5}{\tau^2}} \tag{10}$$

$$I_a = I_1 - I_2 = \frac{1}{\tau} \frac{1}{s + \frac{1}{\tau}} I_1 \tag{11}$$

$$I_b = I_3 - I_4 = \frac{1}{2\tau} \frac{1}{s + \frac{1}{2\tau}} I_1 \tag{12}$$

$$I_c = I_5 = \frac{1}{\tau} \frac{1}{s + \frac{1}{\tau}} I_1 \tag{13}$$

$$I_R = I_2 = \frac{s}{s + \frac{1}{\tau}} I_1 \tag{14}$$

In the time domain

$$i_L = \frac{3}{10} \frac{\phi}{L_1} (1 + 8.9e^{-\frac{8.4}{\tau} t} + 0.1e^{-\frac{0.6}{\tau} t}, \tag{15}$$

$$i_a = i_c = \frac{3}{10} \frac{\phi}{L_1} (1 - 1.2e^{-\frac{8.4}{\tau} t} + 0.25e^{-\frac{0.6}{\tau} t} - 0.05e^{-t/\tau}) \tag{16}$$

$$i_b = \frac{3}{10} \frac{\phi}{L_1} (1 - 0.56e^{-\frac{8.4}{\tau} t} - 0.5e^{-\frac{0.6}{\tau} t} + 0.06e^{-t/2\tau}) \tag{17}$$

$$i_R = \frac{3}{10} \frac{\phi}{L_1} (10e^{-\frac{8.4}{\tau} t} - 0.15e^{-\frac{0.6}{\tau} t} + 0.05e^{-t/\tau}) \quad . \tag{18}$$

Eqs. (15) - (18) are plotted in Fig. 7 with τ as a parameter. It is seen that for $\tau = 0.5$ sec. and a pumping speed of 20ϕ per sec., the current in the storage inductors reaches approximately 60% of its peak value just before the next stroke of flux pumping. In other words, if the time constant is not short enough compared to the

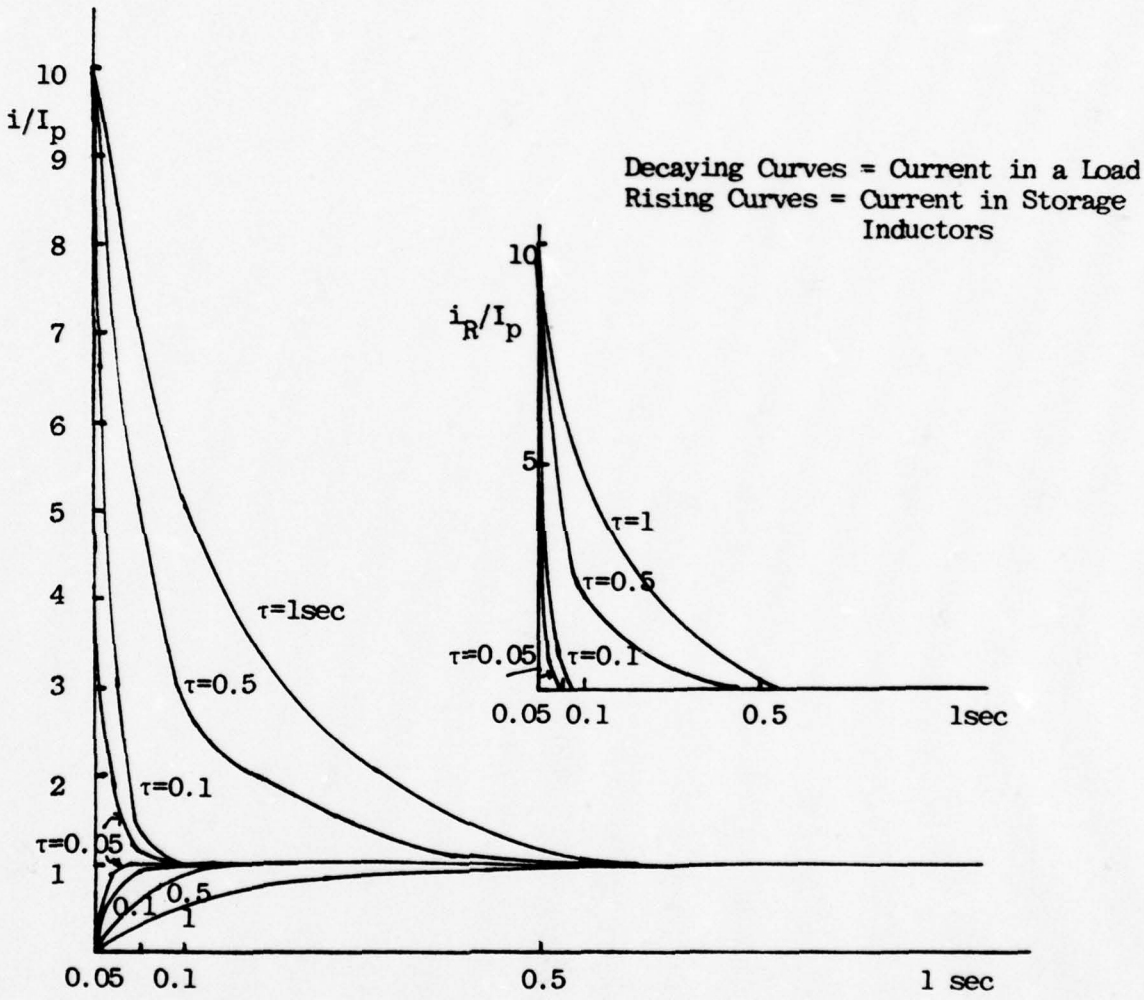

Fig. 7 Charging Characteristics of SKRAM Generator for Different values of $\tau = \frac{L_1}{R}$. Curves in the Insert Show currents in the Switches. I_p refers to the steady state current $\frac{3}{10}\frac{\Phi}{L_1}$ induced in the inductors at each stroke of flux pumping.

pumping period, a good part of magnetic flux pumped into the circuit builds up in the load inductor instead of the storage inductors momentarily, which will give rise to a high transient current in the load. The insert in Fig. 7 shows the dependence of the current in the switches on the time constant. This transient current will result in an energy loss of the system through the power dissipation on the switches. The requirement for the time constant τ for the fast response of the system is given roughly by the inequality $\tau = L_1/R \leq 2T$, where T is the period of flux pumping.

B. Discharging Period

Similar expressions to those in A are found and are

$$I_L = I_1 = \frac{s + 6/\tau}{s(s+3/\tau)} I_i \tag{19}$$

$$I_a = I_1 - I_2 = \frac{s + 2/\tau}{s(s+3/\tau)} I_i = I_b = I_i \tag{20}$$

$$I_R = I_3 - I_2 = \frac{1}{s+3/\tau} I_i \quad , \tag{21}$$

where I_i is the circulating current in the circuit before discharge. Solving in the time domain,

$$i_L = 2I_i(1 - \frac{1}{2} e^{-3t/\tau}) \tag{22}$$

$$i_a = i_b = i_c = \frac{2}{3} I_i(1 + \frac{1}{2} e^{-3t/\tau}) \tag{23}$$

$$i_R = I_i e^{-3t/\tau} \tag{24}$$

Eqs. (22) - (24) are plotted in Fig. 8 for different time

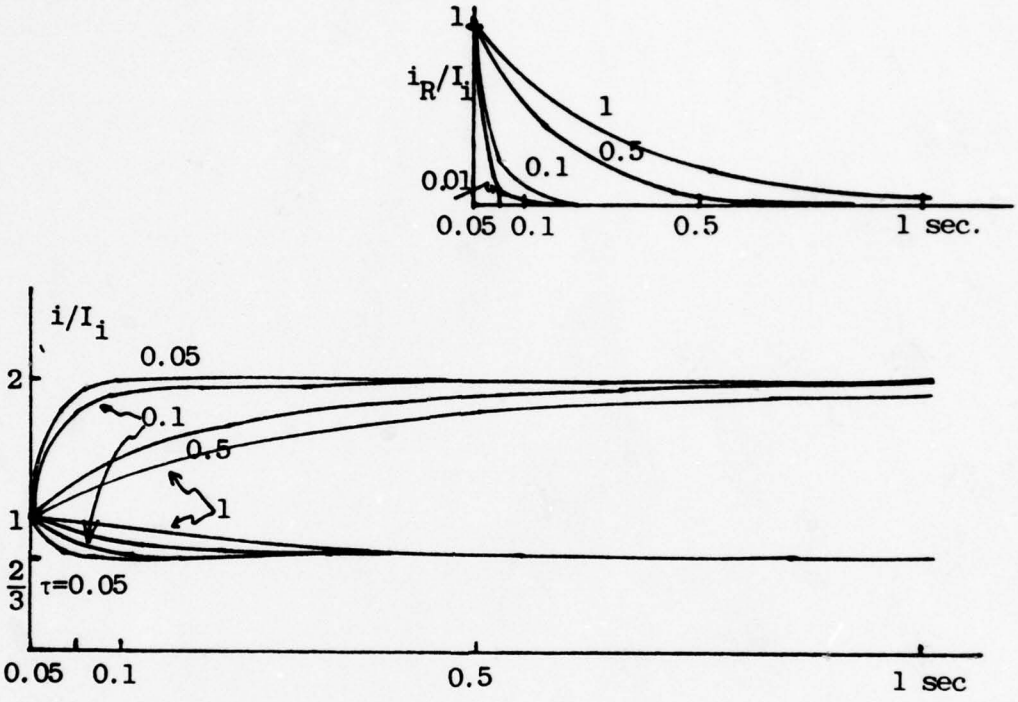

Fig. 8 Discharging Characteristics of SKRAM Generator for Different Values of $\tau = L_1/R$.

constants. It is seen that the current rise time in the load is shortened by 1/3 of the simple transfer scheme. The insert in Fig. 8 shows the current through the switches in the discharging period. The peak current to be handled by switches is equal to the initial current I_i .

In summary, the transient analysis reveals the following characteristics of the SKRAM generator.

1) To prevent a transient build-up of current in a load inductor while the generator is being charged, the resistance of the open switches must be high enough to satisfy the inequality, $\tau = L_1/R \leq 2T$, where T is the flux pumping period.
2) The discharging time constant of the generator is given by $\tau_D = \frac{1}{3}\tau = \frac{1}{3}\frac{L_1}{R}$.
3) Power dissipation and hence energy loss results from the transient current in the switches and depends on τ . The peak voltage developing across the opening switches in discharge is $V_R = RI_i$, where R is the resistance of the switches in open condition.

CHAPTER III

FLUX PUMP

1. Design Consideration

One of the simplest version of the rotating-magnet flux pump is shown in Fig. 9 . It consists of a cylindrical Nb sheet and magnets of a few poles rotating about a concentric shaft to the sheet. The poles of the magnets have the same polarity facing the sheet and produce a magnetic field which is high enough to cause the superconducting Nb sheet to quench to the normal state over a small region. Superconducting wires are connected to the top and bottom of the Nb cylinder periodically and grouped together to form the output terminal of the flux pump.

The operation of the flux pump relies on the principle of flux conservation in a multiply-connected superconductor. Although an exact theoretical prediction has not been successful yet, the following set of equations has been formulated on the basis of phenomenological arguments for the emf and the loss of the flux pump,[23-25]

$$\text{emf} = n\omega(P - L_p I) \tag{25}$$

$$\text{loss} = n\omega L_p I_o^2 \tag{26}$$

where n is the number of poles of the rotor, ω the rotation speed in rps, I the load current, P the flux per normal spot, and L_p and I_o are the effective inductance of the spot, and the effective

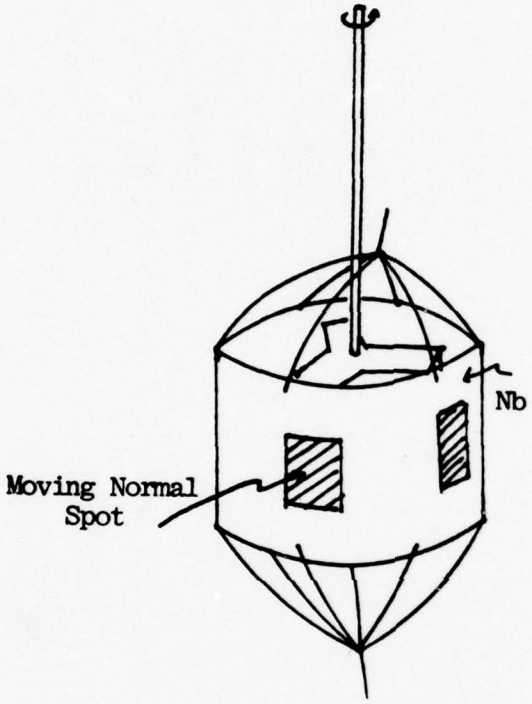

Fig. 9 A Rotating-Magnet Type Flux Pump.

current on the spot, respectively. However, because of the complicated nature of the physics of the moving spot, those effective quantities have not been quantitatively calculated.

A general idea on selecting a proper material suggests that a thin superconducting foil of high resistivity at normal state has a better performance than a sheet of low resistivity for high speed operation. This is due to the fact that a moving normal spot on the superconductor is distorted considerably as the material is thicker and of lower resistivity.[28]

2. Construction Details

The dimension of the Nb sheet cylinder must be designed so as to be able to carry the design current. By a rule of thumb, the current carrying capacity of a pure Nb sheet is estimated to be 10-15 Amp/mm for 1 mil thickness.[29] To secure an efficient operation at high speed, a thin Nb foil of 0.4 mil thickness is wound as a cylinder of 2.875" diameter, whose circumference is 9". The current carrying capacity is then found to be around 1000 Amps. Twelve NbTi superconducting wires of 0.02" dia. are spot-welded on both edges of the Nb foil. Fig. 10 shows the photograph of the unwound Nb foil with NbTi wires spot-welded. Forming a cylinder with thin foil requires a special consideration in selecting the structural materials. From a series of tests with different materials, it has been found that teflon and micarta have significantly different thermal contraction ratios with each other at low temperature. Therefore, the Nb foil is allowed to fit between the teflon and micarta rings, and when it gets

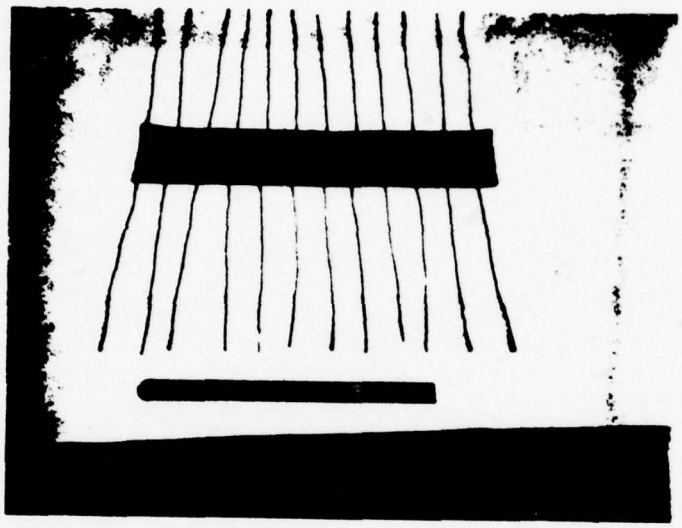

Fig. 10 Photograph of the Unwound Nb Foil with NbTi Wires Spot-Welded.

cold, the outside teflon ring shrinks inward to tightly hold the foil.

Although it depends on many parameters such as its purity and metallurgical process, the critical field of Nb is estimated to be around 2 kG at liquid He temperature. To provide the high magnetic field needed to create the normal spots, two ring type permanent magnets made of Alnico V are inserted at the top and bottom of the rotor. Fig. 11 is a photograph of the rotors with various number of poles together with the ring type permanent magnets. A closed magnetic return path is provided by a mild steel sleeve outside the Nb foil cylinder. The gap between the rotor and the stator is 20 mils. Due to the magnetic flux loss of the permanent magnets during the assembly process, remagnetization is necessary after completing the flux pump assembly. For this purpose, two magnetizing coils have been added to the actual design. By applying a peak current of 25 Amp to the coils for 1 sec., a magnetic field of 4.6 kG is established in the gap. Fig. 12 shows the cross-sectional view of the flux pump, and Fig.13 is a photograph of the completed flux pump.

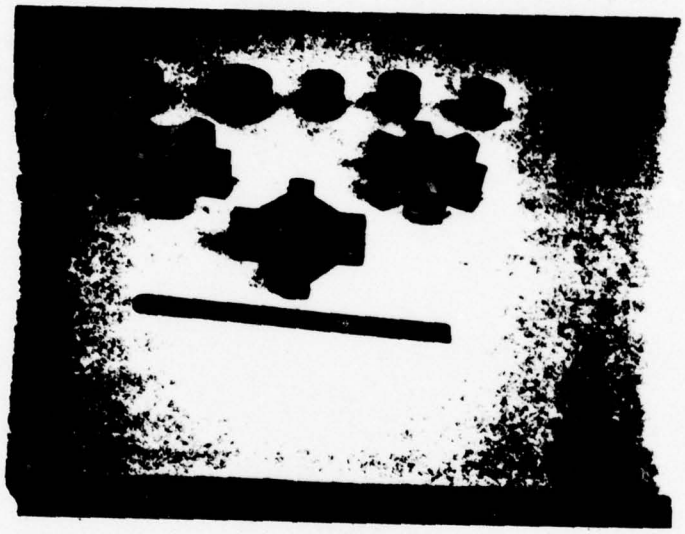

Fig. 11 Photograph of the Rotors with Different Number of Pole Pieces, Together with Ring Type Permanent Magnets.

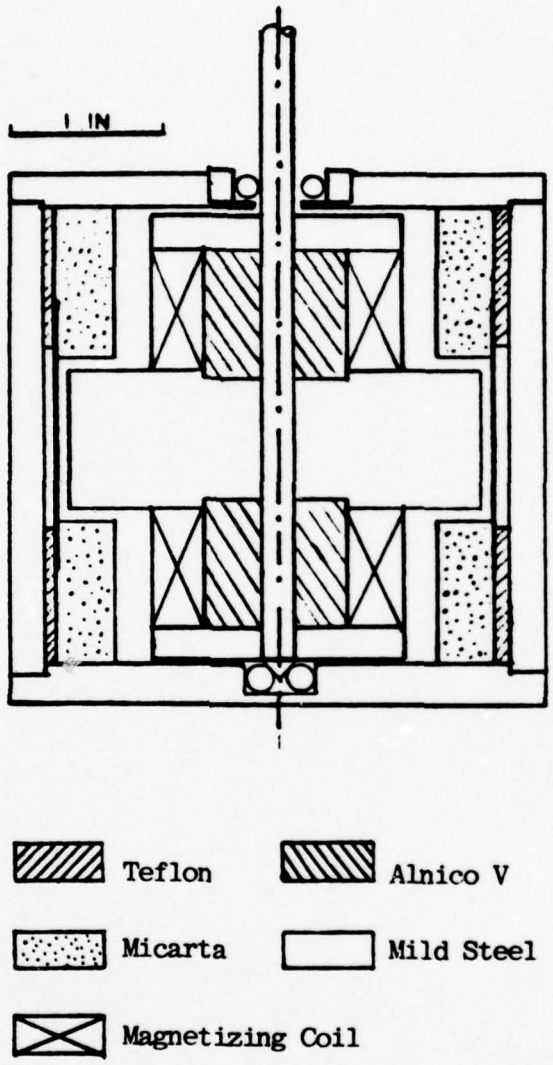

Fig. 12 Cross-Sectional View of Flux Pump.

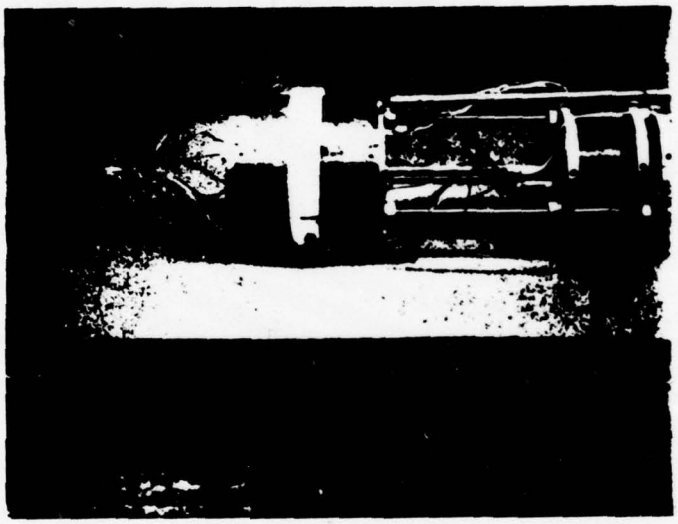

Fig. 13 Photograph of Completed Flux Pump Together with Superconducting Storage Inductors.

CHAPTER IV

EXPERIMENTS

1. Description of Experimental Apparatus

A. Prototype SKRAM Generator System

A prototype superconducting SKRAM generator is shown in Fig. 14. Three storage inductors and one load inductor are made with NbTi superconducting wire wound on the aluminum coil forms of 1" ID, 2" OD, and 1 ½" length. Each layer of the inductors has been impregnated in the epoxy to provide the rigidity of the winding at low temperature. The inductance of each storage inductor is measured to be 18 mH, and the load inductance is 5.6 mH.

The scheme of magnetic switching of the superconducting Nb strip to normal state has been conceived for the superconducting switches. The cross-sectional area and the length of the strip are to be designed to meet the requirements of the high resistance in the normal state and the high current carrying capacity in the superconducting state. For the design current of 20 Amp and the normal state resistance of 0.1 ohm, 0.5 mil thick Nb foil is cut into 1/8" wide and 12" long strips. Each strip is folded several times to fit into the hole of the switching coils. Fig. 15 shows the close-up view of the superconducting switches. One coil contains 4 strips and the other coil contains 2 strips, corresponding to the circuit diagram of Fig. 1 . The magnetizing current in the switching coils is controlled by the SPDT relay control circuit of Fig. 16 . In the charging period of the

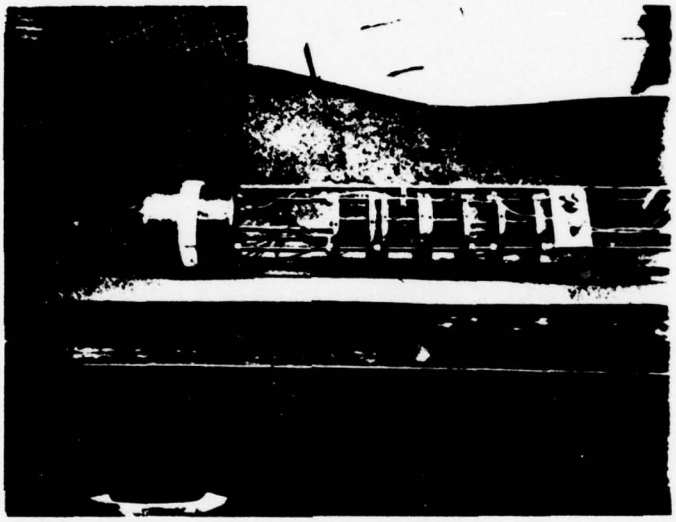

Fig. 14 Photograph of a Prototype Superconducting SKRAM Generator.

Fig. 15 Superconducting Switches

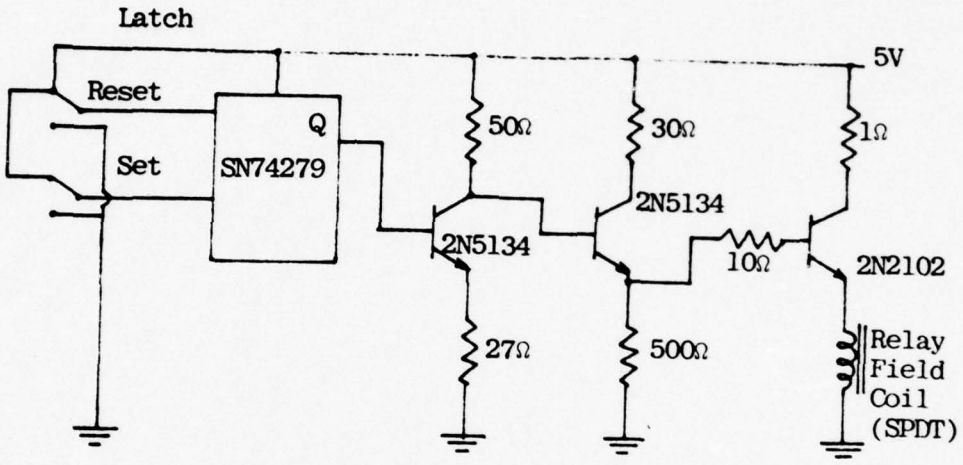

Fig. 16 Relay Control Circuit

generator, the latch output is maintained LOW to energize the relay, and the magnetizing current flows through the switching coil having 4 strips in it. For the discharge, the latch is set to HIGH to release the relay and the current is transferred to the other switching coil with 2 strips. As soon as the magnetic field at the center of the coil exceeds the critical field of Nb, the Nb strips become resistive and the energy transfer takes place.

B. Instrumentation

The quantities to be monitored in the experiments are 1) the temperature inside the liquid He dewar, 2) the liquid He level, 3) the magnetic field in the gap between the rotor and the stator of the flux pump, 4) the emf of the flux pump and 5) the currents in the storage and load inductors.

The temperature is monitored with a transistor RCA 148 by measuring the forward voltage drop across the emitter-base junction for 10μA forward current, which has been calibrated against the temperature sensing diode DRC-7*. It is found that the voltage drop of the transistor has a good reproducibility below the liquid nitrogen temperature, and when it reaches the liquid He temperature, the junction becomes a complete open circuit. Several types of switching diodes and carbon resistors have been tested, but any of these does not have such a good reliability as the transistor.

---

*Made by Lake Shore Cryotronics, Inc.

The liquid He level is measured with a liquid He level sensor and Model 110 liquid He level meter made by the American Magnetics, Inc.

The magnetic field in the gap of the flux pump and the currents in the inductors are measured with a transverse and an axial Hall probes made by F. W. Bell, Inc. The transverse Hall probe has been inserted in the gap during the assembly process of the flux pump. The currents in the storage inductors and the load inductor are measured by detecting the magnetic field at the center of the inductors with separate axial Hall probes, which have been calibrated with known currents. Fig. 17 is a photograph of the transverse and axial Hall probes together with a temperature sensing transistor.

C. Experimental Procedures

Fig. 18 shows the schematic view of the apparatus put into the liquid He dewar. Before the cooling process, dry gaseous He is used to purge out all the air inside the dewar to prevent the air from freezing around the bearing and the other moving parts. The latent heat of the liquid He is as small as 0.65 cal/cm^3, compared to 38.6 cal/cm^3 for the liquid nitrogen. The specific heat of most of the metal decreases as the temperature is lowered. Therefore, precooling of the system down to the liquid nitrogen temperature precedes the liquid He transfer by filling the outer dewar with the liquid nitrogen and allowing heat transfer through the gaseous nitrogen layer between the inner and outer dewars. It takes about 4-5 hours to completely cool down to 77.3°K. After the precooling, the nitrogen gas layer

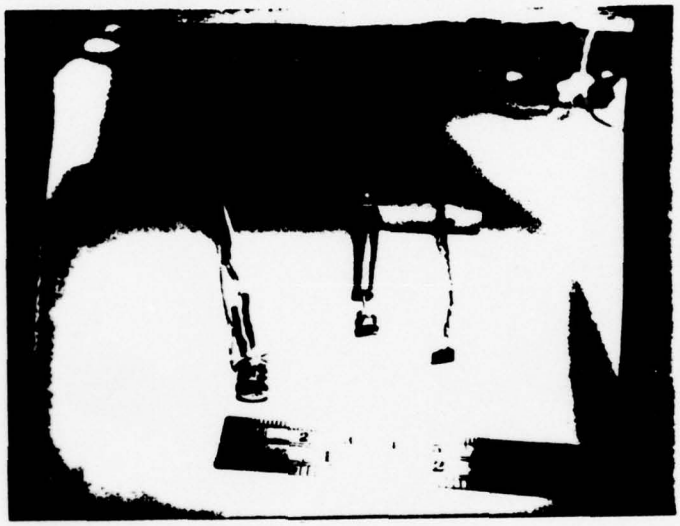

Fig. 17 Axial and Transverse Hall Probes Together with a Temperature Sensing Transistor.

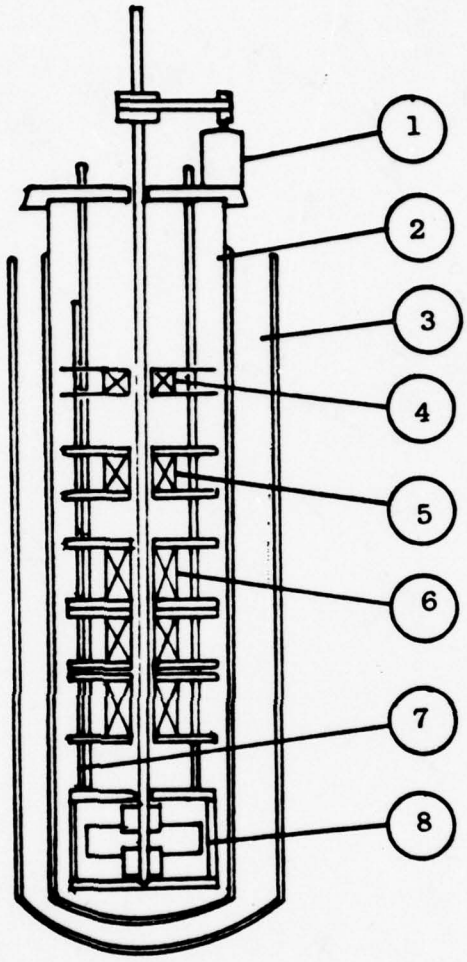

Fig. 18 A Schematic Representation of Experimental Apparatus.

(1) Motor (2) Liquid He Dewar (3) Liquid Nitrogen Dewar (4) Switching Coil (5) Load Inductor (6) Storage Inductor (7) Liquid He Level Sensor (8) Flux Pump.

begins to be evacuated. With a liquid nitrogen cold trap, the diffusion pump can pump out the nitrogen gas down to 10^{-6}torr within 2 hours. Fig. 19 shows the photograph of the dewar with the motor installed on top of it. The rubber stopper on the side neck is to release the heavy pressure arising from the vaporizing helium. He is transferred via vacuum-jacketed flexible transfer line made of stainless steel. The transfer rate is controlled by the pressure in the liquid He container, which can be adjusted with the external pressurizing gaseous He. About 3-4 lb of pressure is necessary to continue transferring. Fig. 20 is a photograph of the liquid He transfer process.

2. Measurements

First, the flux pump was tested with one storage inductor to see its performance characteristics. The normal spot size is 3.32 cm^2 and the magnetic field at the center of the spot is 4.6 kG. Fig. 21 shows an oscilloscope display of the magnetic field variation in the gap (a) at room temperature and (b) at the liquid He temperature as the rotor rotates. Observations have been made for different rotation directions and it has been confirmed that the nonuniformity of the magnetic field is not due to the geometry of the pole face but due to the eddy currents induced around the moving spot. With a rotation speed of 120 rpm, the current induced in the storage inductor reached 18 Amp after 5 min. operation, and it showed a linear increase up to 110 Amp, the critical current of the NbTi superconducting wire. In fact, the current increase in the storage inductor is a discontinuous

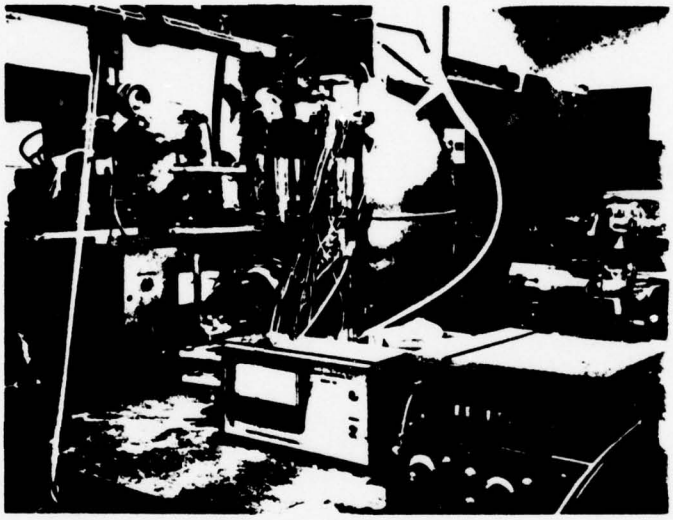

Fig. 19 Photograph of the Liquid He Densor, also Showing the Motor Mount and the Pressure Release Rubber Stopper Arrangement.

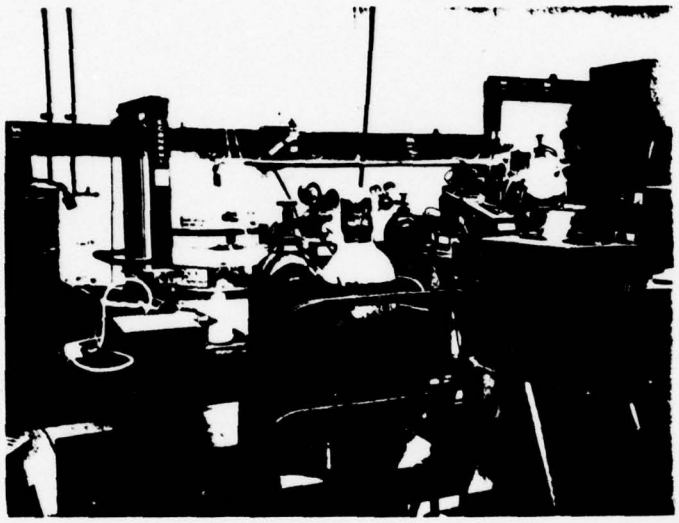

Fig. 20 Liquid He Transfer

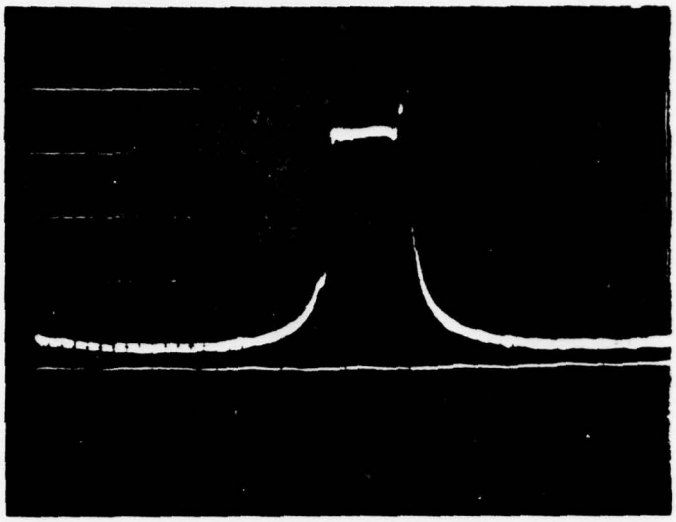

(a) Ver. 1 mV/cm, Hor. 10 ms/cm.

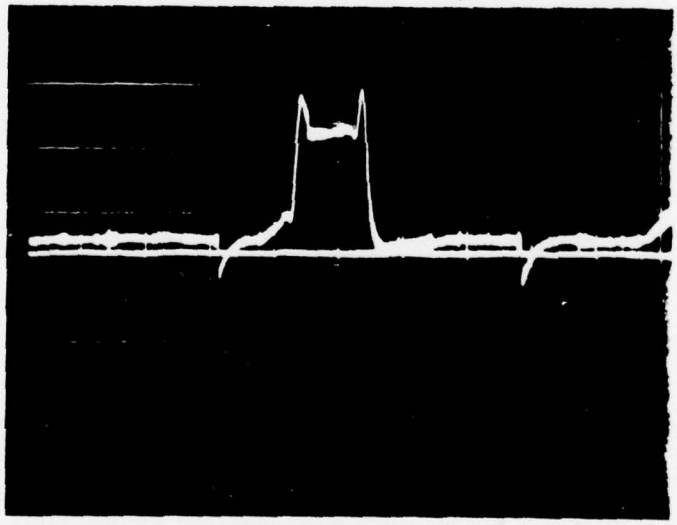

(b) Ver. 2 mV/cm, Hor. 10 ms/cm.

Fig. 21 The Magnetic Field Variation in the Gap while the Rotor Rotates. (a) At Room Temperature and (b) At the Liquid He Temperature.

process, as is evident from the oscilloscope picture of the emf of the flux pump in Fig. 22. It is seen that the flux pumping occurs once in every $\frac{1}{nx\omega}$ sec., where n is the number of poles and ω is the rotation speed in rps. The emf was measured by AC voltmeter for different rotation speeds as in Fig. 23. It shows a deviation from the linear increase of emf at high speed range, owing to the degradation of the moving normal spot at high speed operation.

After the flux pump test, the entire SKRAM generator system was tested. Table 1(a) and (b) summarize the charging and the discharging test results. Due to the small current carrying capacity of the Nb foil superconducting switches, the test was performed in the current range of 10-20 Amp. The first three columns in (a) shows the current rise in both storage and load inductors while the flux pump was running at 120 rpm, and the last two columns are the currents approaching the steady state after the flux pump stopped pumping. It is seen that the resistance of the Nb foil switches was not high enough to prevent the transient build up of current in the load inductor. In Table 1(b), the current changes in the load inductor due to the switching are shown at various situation. When the generator was discharged just after the flux pump stopped, the current amplification obtained was 1.5. When the discharge was done after the system reached steady state, it approaches 1.8 which is very close to the theoretical prediction of 2 . The difference of currents between the original value and the value after the generator returned to the charging

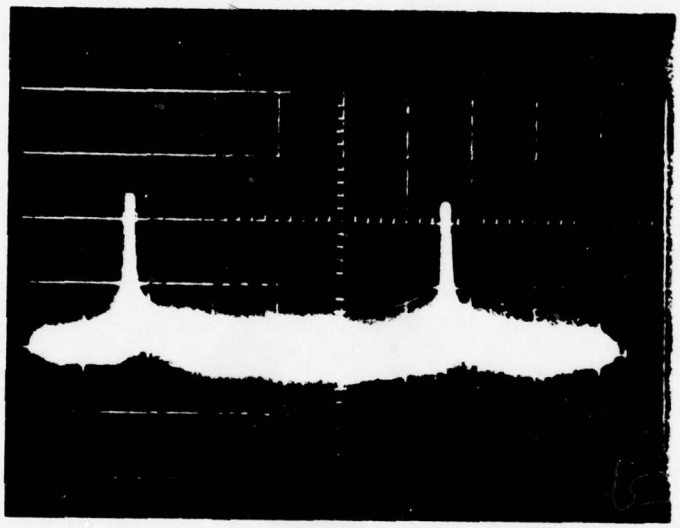

Fig. 22 The emf of the Flux Pump at 80 rpm.
Ver. 2mV/cm. Hor. 50 msec/cm.

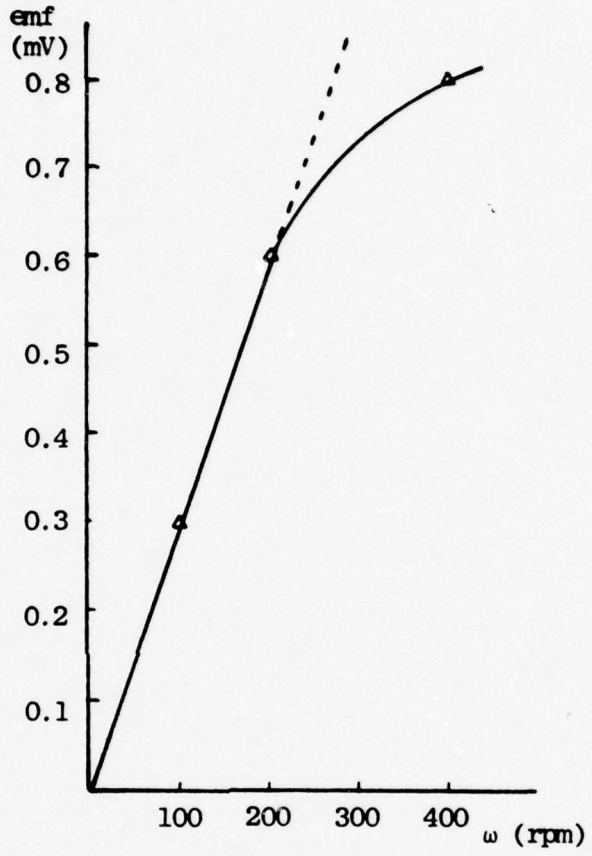

Fig. 22 The emf vs. Rotation Speed, Measured by AC Voltmeter.

Time / Current	Flux Pump Running			After Charge up	
	5 min	8 min	10 min	5 min	10 min
I_2 (Amp)	6.59	9.72	12.22	9.09	7.84
I_1 (Amp)	5.03	6.37	7.70	7.70	6.70
I_2/L_1	1.31	1.52	1.59	1.18	1.17

(a) The currents in the load and storage inductors during the charging period, where I_2 is the load current and I_1 is the current in the storage inductors.

Discharge	Before Discharge (Amp)	Discharge (Amp)	Return to Original (Amp)	A
Just After Charge up	10.97	16.59	8.47	1.51
3 min. after Charge up	10.34	17.54	7.84	1.73
10 min. after Charge up	7.84	14.09	7.22	1.80

(b) The current amplification in the load inductor after the discharge.

Table 1. Experimental Results of the Charging and the Discharging Test of the SKRAM Generator.

configuration resulted from the power dissipation on the switches. It was observed that for a flux pump rotation speed of 300 rpm, the current rise in the load inductor was much faster than that in the storage inductor. The discharge switching time was observed to be around 10 msec.

CHAPTER V

DISCUSSION AND CONCLUSIONS

The superconducting SKRAM generator is shown to be a feasible scheme to generate a high current out of the magnetic energy stored in many inductors. Compared to the simple inductive energy storage system, it has the following features.

1) The maximum efficiency of energy transfer is 33%.
2) The current to be handled by the switches is less than the current generated in the load inductor.
3) The discharge time is shorter by a factor of 1/n, where n is the number of the storage inductors.

As shown in the transient analysis and the experimental test results, the normal state resistance of the superconducting switches determines the transient condition of the system not only in the discharging period but in the charging period. When the time constant is too large compared to the pumping period in the charging period, a high transient current builds up in the load inductor, and a good part of the energy is lost through the power dissipation on the switches. In the discharging period, it limits the fast delivery of energy to the load. In the prototype SKRAM generator, the Nb strip switches could not be made to have a resistance higher than 0.1 ohm due to the space limitation. To increase the resistance of the switches with a designed current carrying capacity, the length of

the strips must be increased, which may be impractical in quenching the superconductivity with a magnetic field in the solenoid. The Nb wire would be better than the strips in increasing the length and also in removing the fringe effect as present in the strip switches. However, it is not commercially available yet. One suggestion is to make use of a thin film superconductor deposited on a coaxial form, but further study has to be made for the design parameters, since the thin film superconductor has different characteristics from the bulk superconductor.

The flux pump built in this work has a good performance characteristic up to 400 rpm rotation. To further improve the efficiency at high speed, the idea of substituting a thin film of Nb for the foil has been suggested. One of the disadvantages that the present design of the flux pump has is the high cost of initial cooling due to the heavy weight of the mild steel sleeve and the other accessories used for the magnetic return path. If the electromagnets are substituted for the permanent magnets, the overall weight is expected to reduce substantially.

In the experimental procedures, precooling of the system down to the liquid nitrogen temperature turned out to be a very important procedure to effectively make use of the liquid He in reaching the superconducting state. The pressure in the vacuum layer between the liquid He and the liquid nitrogen is to be ensured to be low enough to provide a good thermal insulation.

APPENDIX I

1. Charging Period

Referring back to Fig. 6(a), the following set of simultaneous equations is obtained in the frequency domain for the charging circuit of the SKRAM generator.

$$(\tfrac{4}{3}\,sL + 2R)I_1 - sLI_2 - RI_3 - RI_5 = s\Phi \qquad \text{(I-1)}$$

$$-sLI_1 + (sL + R)I_2 = 0 \qquad \text{(I-2)}$$

$$-RI_1 + (sL + R)I_3 - sLI_4 = 0 \qquad \text{(I-3)}$$

$$-sLI_3 + (sL + R)I_4 = 0 \qquad \text{(I-4)}$$

$$-RI_1 + (sL + R)I_5 = 0 \qquad \text{(I-5)}$$

where $L = L_i$.

From Eqs. (A-2) - (A-5), the relations between the loop currents are found to be as

$$I_2 = \frac{s}{s + \frac{1}{\tau}}\, I_1 \qquad \text{(I-6)}$$

$$I_3 = \frac{1}{2}\,\frac{s + \frac{1}{\tau}}{s + \frac{1}{2\tau}}\, I_1 \qquad \text{(I-7)}$$

$$I_4 = \frac{s}{s + \frac{1}{\tau}}\, I_1 \qquad \text{(I-8)}$$

$$I_5 = \frac{1}{\tau}\,\frac{1}{s + \frac{1}{\tau}}\, I_1 \qquad \text{(I-9)}$$

where $\tau = L/R$.

Substituting Eqs. (A-6) - (A-9) into Eq. (A-1) , I_1 is given by

$$I_1 = \frac{3\phi}{L} \frac{s^2 + \frac{3}{2\tau} s + \frac{1}{2\tau^2}}{s^2 + \frac{9}{\tau} s + \frac{5}{\tau^2}} \qquad \text{(I-10)}$$

In the time domain, I_1 is transformed into $i_1(t)$ as

$$i_1(t) = \frac{3\phi}{10L} \left(1 + 8.9e^{-\frac{8.4}{\tau} t} + 0.1e^{-\frac{0.6}{\tau} t}\right) \qquad \text{(I-11)}$$

Applying the convolution theorem to Eqs. (A-6) - (A-9) , all the loop currents can be obtained in the time domain as follows

$$i_2(t) = \frac{3}{10} \frac{\phi}{L} \left(10e^{-\frac{8.4}{\tau} t} - 0.15e^{-\frac{0.6}{\tau} t} + 0.05e^{-t/\tau}\right) \qquad \text{(I-12)}$$

$$i_3(t) = \frac{3}{10} \frac{\phi}{L} \left(1+9.46e^{-\frac{8.4}{\tau} t} - 0.65e^{-\frac{0.6}{\tau} t} + 0.05e^{-t/\tau} + 0.06e^{-t/2\tau}\right) \qquad \text{(I-13)}$$

$$i_4(t) = i_2(t) \qquad \text{(I-14)}$$

$$i_5(t) = \frac{3}{10} \frac{\phi}{L} \left(1-1.2e^{-\frac{8.4}{\tau} t} + 0.25e^{-\frac{0.6}{\tau} t} - 0.05e^{-t/\tau}\right) \qquad \text{(I-15)}$$

2. Discharging Period

A similar set of equations is obtained for the discharging circuit of Fig. 6(b).

$$\frac{4}{3} sLI_1 - sLI_2 = \frac{4}{3} LI_i \tag{I-16}$$

$$-sLI_1 + (sL + R)I_2 - RI_3 = -LI_i \tag{I-17}$$

$$-RI_2 + (sL + R)I_3 - sLI_4 = LI_i \tag{I-18}$$

$$-sLI_3 + (sL + R)I_4 - RI_5 = -LI_i \tag{I-19}$$

$$-RI_4 + (sL + R)I_5 = LI_i \tag{I-20}$$

where I_i is the persistent current around the circuit. Solving the above equations simultaneously, it is found that

$$I_1 = \frac{s + 6/\tau}{s(s + 3/\tau)} I_i \tag{I-21}$$

$$I_2 = \frac{4/\tau}{s(s + 3/\tau)} I_i \tag{I-22}$$

$$I_3 = \frac{s + 4/\tau}{s(s + 3/\tau)} I_i \tag{I-23}$$

$$I_4 = \frac{2}{\tau} \frac{1}{s(s + 3/\tau)} I_i \tag{I-24}$$

$$I_5 = \frac{s + 2/\tau}{s(s + 3/\tau)} I_i \tag{I-25}$$

APPENDIX II

A SCHEME OF HIGH CURRENT GENERATION IN SUPERCONDUCTING MAGNETS

This is a brief note on a new scheme of achieving a high current generation in a superconducting magnet with a modified version of the SKRAM generator. It is shown in Chapter II that the SKRAM generator can obtain a maximum current amplification of $1 + L_1/L_2$ when a large number of inductors are employed. By modifying the circuit and charging the system repetitively, it is shown below that the current amplification equal to the number of inductors can be attained.

One more switch is added in shunt with the load inductor as shown in Fig. II-1 . The method of operation is the same as that in the SKRAM generator except that the procedures repeat and the load inductor is not included in the charging path.

1) Close the switches S's and open the switches S_1's.
2) The series of inductors are charged by the flux pump, and a persistent current I_i is made to circulate around the circuit.
3) The switches S_1's are now closed, and then S's are open.

Then the current induced in the load inductor is given by the condition of flux conservation in the loop ℓ' as

$$(L_2 + L_1/n)I_{f1} = L_1 I_i \qquad \text{(II-1)}$$

Now, repeat the process 1) to 3) and after the j^{th} iteration, the relation between the load currents at j^{th} and $(j-1)^{th}$ iteration is found to be as

$$(L_2 + L_1/n)I_{fj} = L_1 I_i + L_2 I_{j-1} \qquad \text{(II-2)}$$

From the Eqs. (II-1) and (II-2), I_{fj} is obtained as

$$I_{fj} = r \sum_{k=1}^{j} \frac{n^k}{(n+r)^k} I_i \quad , \qquad \text{(II-3)}$$

where $r = L_1/L_2$. For $j \to \infty$,

$$I_f = nI_i \qquad \text{(II-4)}$$

Therefore, the final current increases n times greater than the circulating current I_i in the storage inductor. The rate of convergence to the final current I_f is determined by the ratio $n/(n+r)$, which is always greater than 1 . For $r > n$, $n/(n+r) < \frac{1}{2}$ and I_{fj} converges to the final value I_f very fast.

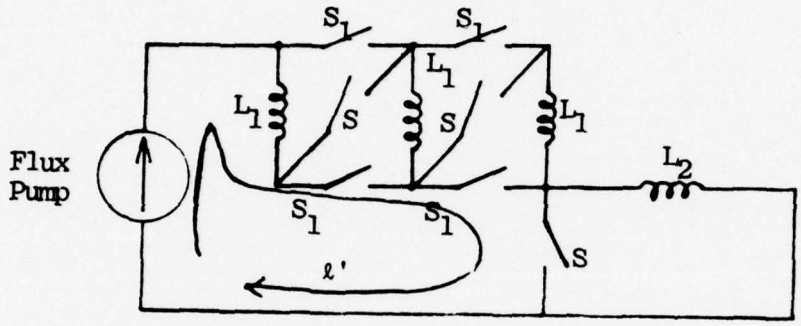

Fig. II-1 Modified SKRAM Generator for High Current Amplification.

REFERENCES

1. Boom, R. W., McIntosh, G. E., Peterson, H. A., and Young, W. C., "Superconducting Energy Storage", Advances in Cryogenic Engineering, Vol. 19, pp. 117, 1974.

2. Cnare, E. C., Cowan, M., Tucker, W. K., Leihser, W. B., and Wesenberg, D. L., "Terawatt Pulse Power Systems Utilizing Inductive Storage", Proceedings of IEEE International Pulsed Power Conference, Lubbock, Texas, Nov. 1976.

3. Komarek, P., "Superconducting Magnets in the World of Energy, Especially in Fusion", Cryogenics, Vol. 16, No. 3, pp. 139, 1976.

4. Early, H. C. and Walker, R. C., "Economics of Multimillion-Joule Inductive Energy Storage", Trans. of the Amer. Inst. of Electrical Engineers, Vol. 76, Part I, pp. 320, 1957.

5. Carruthers, R., "The Storage and Transfer of Energy", High Magnetic Fields, ed. by Kolm, The MIT Press, pp. 307, 1962.

6. Komarek, P. and Ulbricht, A., Proceedings of International Conference on Magnet Technology, Rome, pp. 313, 1975.

7. Laquer, H. L., "Superconducting Magnetic Energy Storage", Cryogenics, Vol. 15, No. 2, pp. 73, 1975.

8. Session IA and IB of the Proceedings of IEEE International Pulsed Power Conference, Lubbock, Texas, Nov. 1976.

9. McFee, R., "Optimum Input Leads for Cryogenic Apparatus", Rev. Sci. Instr., Vol. 30, No. 2, pp. 98, 1959.

10. Williams, J. E. C., "Counterflow Current Leads for Cryogenic Applications", Cryogenics, Vol. 3, No. 12, pp. 234, 1963.

11. Van Beelen, H., et al., "Flux Pumps and Superconducting Solenoids", Physica, Vol. 31, pp. 413, 1965.

12. Hildebrandt, A. F., Elleman, D. G., Whitmore, F. C. and Simkons, R., "Some Experimental Consequences of Flux Conservation within Multiply-Connected Superconductors", J. Appl. Phys., Vol. 33, No. 7, pp. 2375, 1962.

13. Olsen, J. L., "Superconducting Rectifier and Amplifier", Rev. Sci. Instr., Vol. 29, No. 6, pp. 537, 1958.

14. Buchhold, T. A., "Superconductive Power Supply and Its Application for Electrical Flux Pumping", Cryogenics, Vol. 5, No. 8, pp. 212, 1964.

15. Laquer, H. L., "An Electrical Flux Pump for Powering Superconducting Magnet Coils", Cryogenics, Vol. 4, No. 3, pp. 27, 1963.

16. Marchand, J. F. and Volger, J., "Radiation-Induced Transport of Magnetic Flux along a Superconducting Sheet", Phys. Letters, Vol. 2, pp. 118, 1962.

17. Van Beelen, et al., "Experience with Superconducting Coils Fed by Flux Pumps", Proc. of the Conf. on the Physics of Type II Superconductivity, Vol. 2, pp. IV-53, Cleveland, Ohio, 1965.

18. Wipf, S. L., "A Superconducting Direct-Current Generator", Advances in Cryogenic Engineering, Vol. 9, pp. 342, 1964.

19. Volger, J., "The Generation of Heavy Currents in Sperconducting Circuits", Advances in Cryogenic Engineering, Vol. 10, pp. 98, 1965.

20. Van Beelen, H., et al., "A 25000 Gauss, 175 Amperes Nb-25% Zr Wire Magnet Fed by a Flux Pump", Physics Letters, Vol. 7, No. 3, pp. 175, 1963.

21. Lubell, M. S. and Wipf, S. L., "A Cable-Wire Magnet Powered by a Flux Pump", Advances in Cryogenic Engineering, Vol. 13, pp. 150, 1967.

22. Newhouse, V. L., "On Minimizing Flux Pump Heat Dissipation", IEEE Trans. Magnetics, Vol. MAG-4, No. 3, pp. 482, 1968.

23. Wipf, S. L., "Flux Pumps as Power Supplies for Superconducting Coils", Proc. of the International Symposium on Magnet Technology, Stanford, pp. 615, 1965.

24. Van Houwelingen, D. and Volger, J., "The Superconducting-Dynamo Properties and Applications", Philips Res. Reports, Vol. 23, pp. 249, 1968.

25. Voigt, H., "Eine Untersuchung der Vorgange in Supraleitenden Flusspumpen", Z. Natur., Vol. 21a, pp. 510, 1966.

26. Van Beelen, H., et al., "Remarks on a Moving Flux Experiment in Superconducting Sheets", Physica Vol. 36, pp. 107, 1967.

27. Wipf, S. L., "The Case for Flux Pumps and Some of Their Problems", Proc. 1968 Summer Study on Superconducting Devices, BNL50155 (C-55) pp. 632.

28. Van Suchtelen, J., Volger, J. and Van Houwelingen, D., "The Principle and Performance of a Superconducting Dynamo", Cryogenics, Vol. 5, No. 10, pp. 256, 1965.

29. Wipf, S. L., "A 50 kA Flux Pump for the Superconducting Transmission Line Testbed", Los Alamos Int. Report, 1974.

30. Mawardi, O. K. and Chung, H. K., "Pulsed Superconducting Inductive Storage Systems", Proc. of IEEE International Pulsed Power Conference, Lubbock, Texas, Nov. 1976.

PART IV

A SUPERCONDUCTING PULSE GENERATOR

by

LEO HOLLAND

CHAPTER I

INTRODUCTION

1. Problem Statement

Superconducting inductive storage has been receiving much attention recently as developments have made it more economically attractive.[1-4] One of the major goals of this work is construction of various energy storage systems[5] such as load leveling in power systems[6] or pulsed power supplies for devices requiring either a pulsed magnetic field as does the θ-pinch fusion work[7] or an energy pulse as does a pulsed laser system. It is to realize a pulsed power supply utilizing both superconducting inductors and capacitors that this project is directed.

Several difficulties are encountered when an inductive storage system is used for pulsed power applications.[8,9] Two of the major problems are the efficient transfer of energy or current into partially reactive loads and the difficulty in construction of fast acting superconducting switches.[10] To overcome these problems a proposal was made to use a lumped transmission line scheme involving one switch to generate a pulse with near ideal efficiency.[11]

A diagram of a six section pulse generator of the transmission line type is shown in Figure 1. The major disadvantage of this system is that the energy storage rating of the capacitors must equal that of the inductors, thus the utilization of storage capacity is

sacrificed for the gain in energy efficiency over a simple inductor scheme for some loads. This transmission line scheme offers more control over the duration and voltage of the pulse than does the simple inductor. The advantages of this system increase in those cases where the load is not purely resistive, the energy transfer efficiency to a partially reactive load and the peak current for a purely reactive load are higher.

The transmission line model pulse generator retains the simplicity of design of the single inductor storage scheme. It has all passive components and retains the single switch operation, but generates a square rather than exponentially declining pulse. With modifications of the equal values of the inductors and the capacitors along the line or modification of the output stage, the pulse shape can be varied.

2. Selection of System Design

The transmission line model was decided upon after room temperature test of high impedance lines showed that the pulse generated was square and the energy transfer efficiency was near ideal. Improvements on the line design through tapering into time limited filter form was considered but because a larger percentage of the energy storage capacity is not utilized it was deemed a less desirable choice for power applications.

Both of these approaches, transmission line model and time limited filter model, offer a combination of versatility and simplicity. Versatility in that the pulse generated can be of any desired

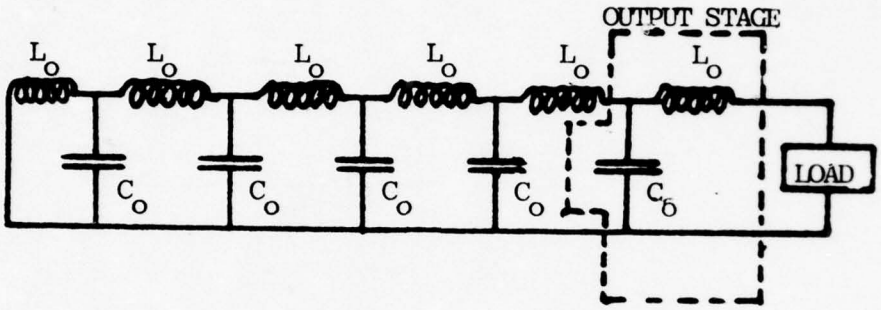

Figure 1. Lumped Parameter Transmission Line Model.

voltage, current and time length, within the physical constraints of construction. Simplicity in that all the elements are passive components and the pulse is generated with the operation of one switch. With the versatility in voltage output of this system and recent work being done with high voltages inside cryostats,[12] this system should be capable of producing the voltage output of any pulsed power supply.

Work has been done over the past fifteen years with discrete flux pumps as demonstrated by Laquer,[13] which are devices that transfer magnetic flux from a source external to the cryostat into a superconducting storage system. As the flux pump offers large current amplification, reduction in the size of the leads into the cryogenic system and reduces the power supply requirements for superconducting magnet or storage systems, the pulsed power supply was charged using a discrete flux pump. To reduce the size of the flux pump versus its power rating from the external source to the superconducting storage system, a model with a higher cycling rate than previous versions, which are typically one hertz or much less, was built. The goal of the design was to demonstrate operation of the flux pump at cycling frequencies comparable to typical alternating current power sources. This would reduce power supply requirements as the flux pump could then act as the interface between the direct current superconducting storage or magnet system and the external alternating current power source.

CHAPTER II

PULSE GENERATOR

1. Theory of Operation

The pulse generator design was based on classical transmission line theory[14] using lumped parameter components. For simplicity the "T" model was used with six inductors as shown in Figure 2. Except for the output stage, the system should pass any signal presented to it as a transmission line with a speed determined by the values of the inductors and capacitors. The speed of propagation of a point on a wave along the line is $\sqrt{LC}$ seconds per section where L and C are the values of the inductors and capacitors respectively.

A pulse is generated by realizing the initial condition in Figure 2 given by

A) $I_1 = I_2 = I_3 = I_4 = I_5 = I_6 = I_0$ initial current (1)

B) $V_1 = V_2 = V_3 = V_4 = V_5 = 0$ volts (2)

These initial conditions represent in an ideal transmission line a square wave which upon propagating first from right to left has been reflected at the short. At the time the incident and reflected sections of the wave exactly cancel each other's voltage, the pulse generators initial conditions are met. Starting from the initial conditions, the leading edge of the square propagates into the load

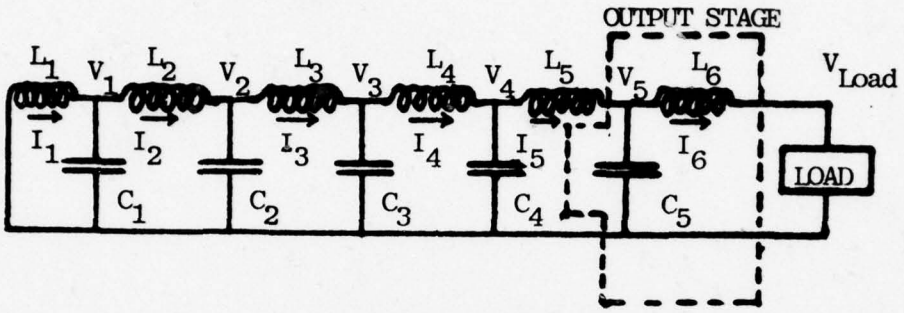

Figure 2. Transmission Line Model Pulse Generator Schematic.

while the trailing edge proceeds right to left, is reflected by the short and then into the load. Thus the load is presented with a pulse of voltage (V_L) given by

$$V_L = 1/2\ I_0 Z_0 \tag{3}$$

where I_0 is the initial current in the inductors and Z_0 is the characteristic impedance of the line given by

$$Z_0 = \sqrt{L/C} \quad . \tag{4}$$

The factor of 1/2 in Eq. (3) comes from the initial current being composed of two parts of a wave traveling in opposite directions. As the pulse at the load begins at the initial time and continues until the trailing edge reaches the load, the pulse lasts for τ seconds given by

$$\tau = 2n\sqrt{LC} \text{ seconds.} \tag{5}$$

The equation for τ is composed of n - the number of sections in the line, $\sqrt{LC}$ - the number of seconds for a point on a wave to propagate through one section and the factor 2 comes from the trailing edge of the pulse traversing each section of the line twice before reaching the load.

2. Realization of the Pulse Generator

To realize the initial conditions necessary for the pulse generator, a switch is added in parallel with the load. As shown in

Figure 3 this switch when closed allows a constant current to flow through all the inductors with no voltage on the capacitors. The pulse is generated by opening the switch whereupon the system is as described in section 2.1 at the initial time.

The current source in series with the switch in Figure 3 was used in the initial demonstration of the principles of the pulse generator. A room temperature test using components as shown in Fig. 3 and a mercury switch was performed to obtain the output shown in Figure 4. The high characteristic impedence of the line, $Z_o = 3x10^4\Omega$, was to overcome the internal resistance of the inductors, 90Ω. The square block in Fig. 4 indicates the ideal pulse from the generator. Results of the room temperature test showed that within the ideal pulse time period of 290 μseconds, approximately 85% of the energy, was delivered to the load. Of the remaining energy ten percent was delivered to the load in the tail of the pulse and the rest was resistive losses inside the inductors.

The capacitor in parallel with the switch in Fig. 3 prevents a 100% overshoot in voltage at the initiation of the pulse. If the load in Fig. 3 is purely resistive, the output inductor would initially generate twice the pulse voltage V_o decaying to V_o within a time constant of one section of the line as shown in Fig. 4. If the load of the pulse generator is purely resistive a simple solution to increasing the match of line to load is to add the capacitor C_L. The capacitor increases the amount of energy contained in the tail of the pulse generated. The optimum value of capacitance for

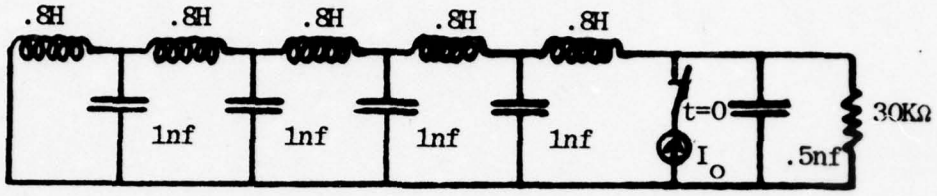

Figure 3. Schematic of Room Temperature Pulse Generator.

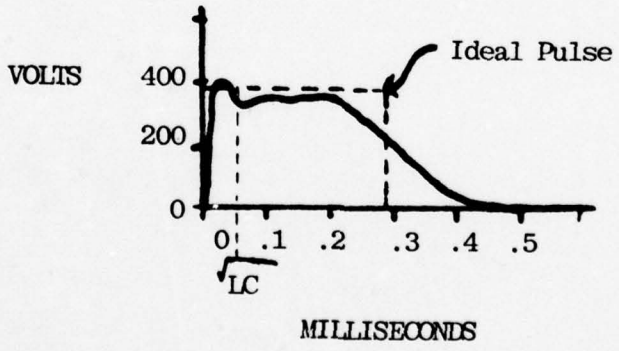

Figure 4. Output Pulse of the Room Temperature Pulse Generator.

C_L to minimize both tail and overshoot is one half the value of the line capacitors. In cases where the load is not purely resistive the output stage must be designed to optimize the pulse shape for the desired application.

3. Comparison of Single Inductor Storage to Pulse Generator

For three specific pulsed load requirements a comparison between the single inductor storage and the lumped transmission line model can be made. The first load requirement is that of efficient energy delivery to a partially inductive load. For the single inductor scheme shown in Figure 5 the energy delivered to the resistive part of the load is given by

$$E_L = 1/2\ L_1 I_o^2 \left(\frac{L_1}{L_1+L_2} \right) \tag{6}$$

where the initial stored energy in L_1 is given by

$$E_S = 1/2\ L_1 I_o^2 \ . \tag{7}$$

A plot of the energy transfer efficiency of this system is shown in Figure 6 graph I for various ratios of load inductor L_2 to storage inductor L_1. Also shown in Fig. 6 graph II is the efficiency of a six section transmission line model pulse generator. This graph is ideal in that it assumes the only loss of energy is that of the output stage inductor charging the load inductor and a square pulse is produced by the remaining sections of the line.

The pulse generator will also reach a higher peak current

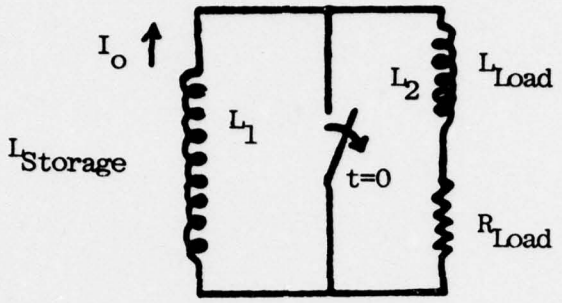

Figure 5. Single Inductor Pulse Generator Scheme.

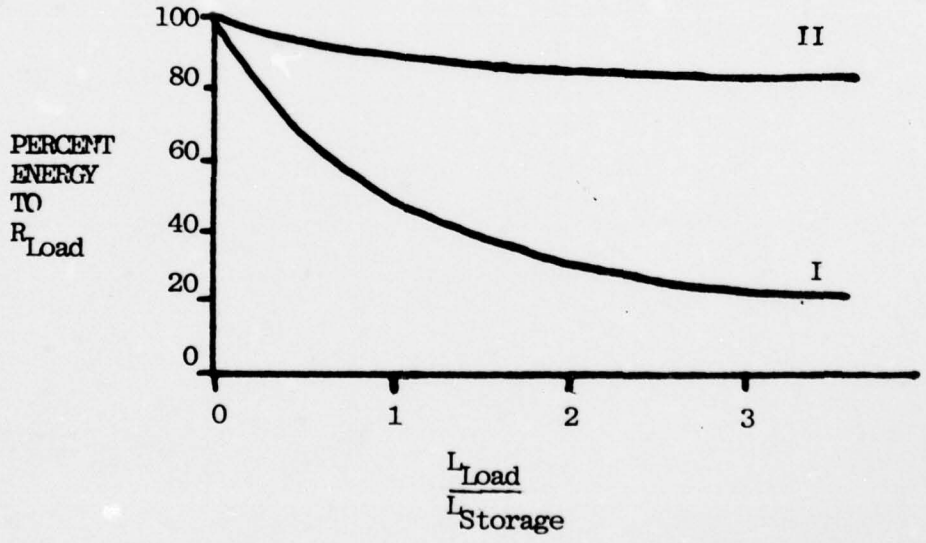

Figure 6. Comparison of Single Inductor, I, and Six Stage Transmission Line, II, Pulse Generators into Partially Inductive Loads.

into a partially inductive load as can be shown by the second load requirement considered, a purely inductive load. For the single inductor storage scheme the current in the load L_2, with the initial current I_o in the storage inductor L_1, will be

$$I = I_0 \frac{L_1}{L_1+L_2} . \tag{8}$$

For equal values of L_1 and L_2 only 25% of the stored energy is delivered to the load. With the pulse generator there will be a comparable inefficiency for the output inductor, but the wave action will allow a peak current in the load equal to the pulse current. Also after the initial voltage generated by the rising current in the load, the load will act as a short reflecting the remaining part of the pulse back into the storage line. If the output switch is closed at an appropriate time, all the energy not lost from the output stage inductor or stored in the load could be recaptured in the superconducting loop.

The third load requirement to be considered is that of a square power pulse. Shown in Figure 7 is the exponential decay curve of either current in a single inductor or voltage in a capacitor being discharged into a resistive load. The optimum fit of a square pulse for energy efficiency is shown in the figure being derived from the equation

$$\frac{d}{dt} (I_0 e^{-t/\tau})^2 Rt = 0 \tag{9}$$

where R is the load resistance and τ the time constant of the system.

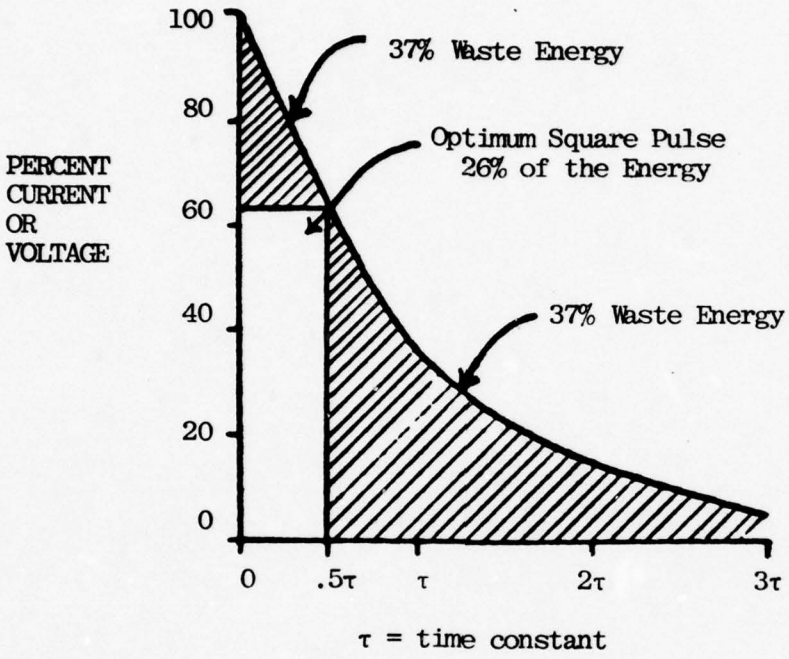

Figure 7. Comparison of Single Inductor or Capacitor versus Transmission Line Scheme Pulse Generator for Square Pulse Load Requirements.

The square pulse of .5τ seconds contains only 26% of the energy stored in the single inductor or capacitor schemes. The transmission line model pulse generator because it generates a square pulse uses 100% of its stored energy to meet the load requirement while adding only 50% unused storage capacity. For repetitive pulse generation with this load requirement, the pulse generator requires one half the total storage capacity and one quarter the energy of a single inductor or capacitor.

4. Design Criterion

From the basic design described, a specific application requires the following information:

a) Impedance of the load - Z_o ,

b) Voltage to the load - V_o ,

c) Duration of the pulse - τ .

To meet these three basic criterion there are four variables

1) Inductance per section - L_o ,

2) Capacitance per section - C_o,

3) Initial current - I_o ,

4) Number of sections - n.

The relationships that must be met by the design are

$$Z_o = \sqrt{L_o/C_o} \quad , \tag{10}$$

$$V_o = 1/2\ I_o\ Z_o \ , \tag{11}$$

$$\tau = 2n\ \sqrt{L_o C_o} \ . \tag{12}$$

With four variables and three constraints theoretically for any given circumstance an infinite number of solutions exist. There are practical restraints on each of the four variables. The current in the largest applications cannot generate fields over 20 Tesla and the inductors and capacitors must be of realizable sizes and numbers. There are restrictions on combinations of variables such as the voltage in Eq. (11) cannot exceed several hundred kilovolts. The number of sections will normally be small though of a sufficient number for efficient generation, that is at least five. A line with a larger n and several switches along the line could be used to generate pulses of different lengths by using only part of the line.

As much work has been and is presently being done with superconducting inductors,[15] no discussion of them will be made in this report. The capacitors used in the experiment were chosen after liquid nitrogen (73°K) tests on several small capacitance types. It was assumed that all oil filled or other capacitors containing liquids would not work at the low temperatures. Tests with tantalum electrolytic type capacitors showed a dielectric break frequency of one kilohertz at 73°K. The tests on disc plate, polystyrene and mylar capacitors were successful with only slight changes in capacitance due to material contractions. Of these types, mylar was chosen because it has the largest capacitance to size ratio. The mylar capacitors used were standard manufacture items and demonstrated a 4% reduction in capacitance at 4.2°K, liquid helium temperature.

The remaining component of the pulse generator is the switch. Work is being done to advance superconducting switch technology, but it is the difficulty and expense of constructing fast acting switches that prompted this design for a pulse generator that uses only one switch. Two means of switching a superconductor to the normal state are exceeding the critical magnetic field or raising the temperature of the material.

Magnetic switches have the advantage of high speed being limited only by electrical time constants in generating the critical field; however, construction of a switch with a low critical field, below 2 Tesla; sufficient critical current, above I_o; and high normal state impedance, greater than ten times the Z_o of the line can be difficult. This is because those materials which have a low critical field, especially type I superconductors, have high electrical conductivities in the normal state such as Niobium at 2×10^8 ℧/m and because of their low critical current densities more bulk is needed to carry a given current. As type I superconductors carry all their current in a surface layer, their use in high impedance switches may be possible with switches made of thin films. The limit on thin film type I switches would be the increasing critical field as the films are made thinner[16] raising the critical field above those easily generated.

Magnetic switching of high normal state resistance type II superconductors also requires generation of high fields such as Niobium-Titanium critical field greater than 10 Tesla. The thermal

switching of a superconductor offers ease in operating high impedance and current switches, but the thermal time constants slow switching to the millisecond range. Placed in contact with or near the superconductor is a normal metal conductor through which a current is passed generating heat and causing the superconductor to exceed its critical temperature.[17] Design considerations for the pulse generator output switch are -1) causing the entire switch to change to the normal state within a time period small compared to the pulse length; 2) thermal time constants in returning to the superconducting state restrict repetition rate of generating pulses; 3) heat generated by the switch can cause a significant loss of helium, latent heat of vaporization 2.6 Joules per milliliter, or a burden on the refrigeration system.

A magnetic switch was the first choice for this project, the switch was to use an etched thin film, 1 μmeter, of Niobium. Niobium was chosen for its high normal state resistivity, 5×10^{-9} Ω-m; high critical field, .2 Tesla, for type I superconductor; and the information readily available about its thin film characteristics. A film with sufficient uniformity and size for the required etching into a zigzag pattern 100 μmeters wide and 10 meters long was not obtained. Therefore as a second choice a thermal switch employing Niobium-Titanium alloy wire in a Cupro-Nickel matrix was constructed.

5. Generator Built and Performance

For a demonstration model of the pulse generator system an

AD-A062 078 CASE WESTERN RESERVE UNIV CLEVELAND OH PLASMA RESEAR--ETC F/G 10/3
THEORETICAL AND EXPERIMENTAL STUDY OF SUPERCONDUCTING INDUCTIVE--ETC(U)
OCT 78 O K MAWARDI, D HAZONY, H K CHUNG AFOSR-76-2886

UNCLASSIFIED AFOSR-TR-78-1500 NL

2 OF 2
ADA
062078

END
DATE
FILMED
3-79
DDC

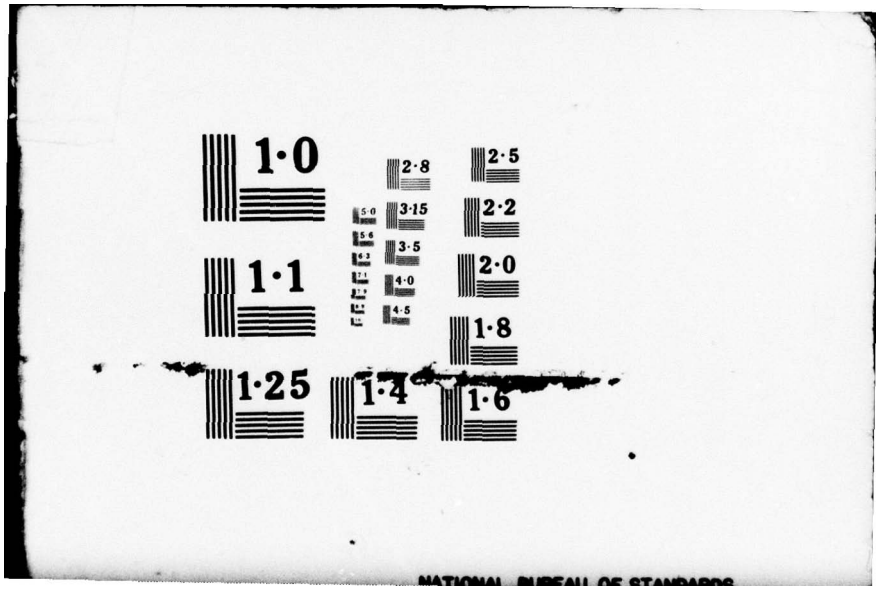
1·0
1·1
1·25
1·4
1·6
1·8
2·0
2·2
2·5
2·8
3·15
3·5
4·0
4·5
5·0

impedance of 33Ω was chosen for convenient voltage levels at low currents and to allow inductors in the millihenery range with the capacitors used. A pulse duration of 2 milliseconds was chosen for ease of instrumentation and for a reasonable number of sections in the line, that is six.

The inductors were constructed of .2 millimeter Niobium - Titanium wire to yield 5 millihenries. The six inductors were mounted on two levels with Mu-Metal magnetic shielding between the layers and the three inductors on each level orthogonal to one another to minimize magnetic coupling. The capacitors were of mylar dielectric type with a nominal capacitance of 5 μfarads. The metal of the capacitors used was not superconducting which in a low impedance line, below 1Ω, may be needed.

The output switch was constructed on an aluminum former identical to those of the inductors. Nichrome wire was wound on the former with an epoxy coating to form a 10Ω heating element. Over the nichrome, .07 millimeter Niobium-Titanium wire in a Cupro-Nickel matrix was wound to form a switch with a normal state resistance of 600Ω. A picture of the assembled pulse generator system is shown in Figure 8 and a schematic in Figure 9.

The pulse generator was operated in the superconducting state under a variety of loads both with and without capacitance in parallel with the load. A diagram of an output pulse into a partially inductive load is shown in Figure 10. The nonsquare shape of the pulse is caused by the initial low resistance of the thermal switch and relatively slow rise in its impedance of $10^5\Omega$ per second. This

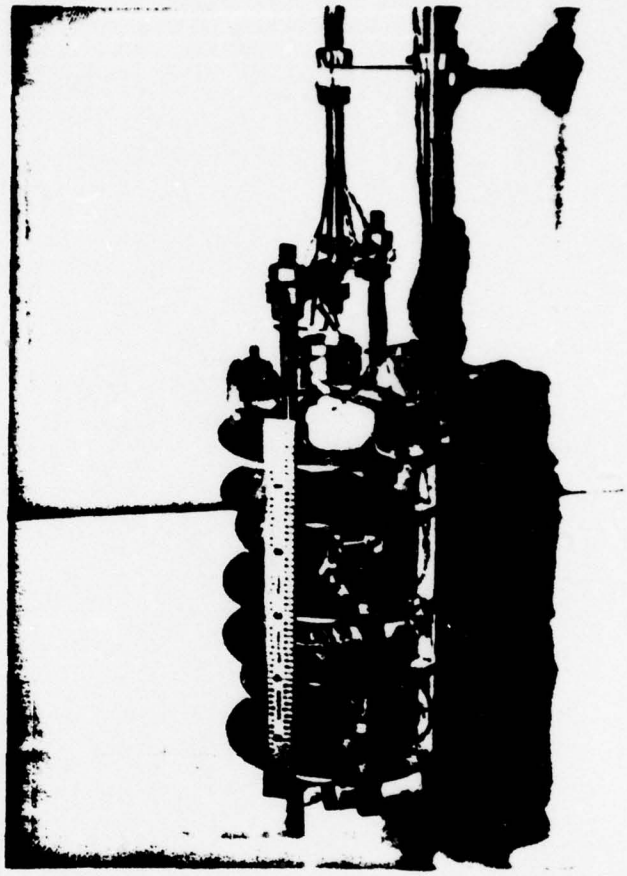

Figure 8. Picture of the Assembled Pulsed Power Supply.

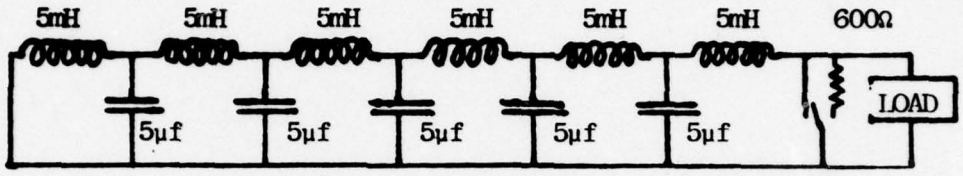

Figure 9. Schematic of the Superconducting Pulse Generator.

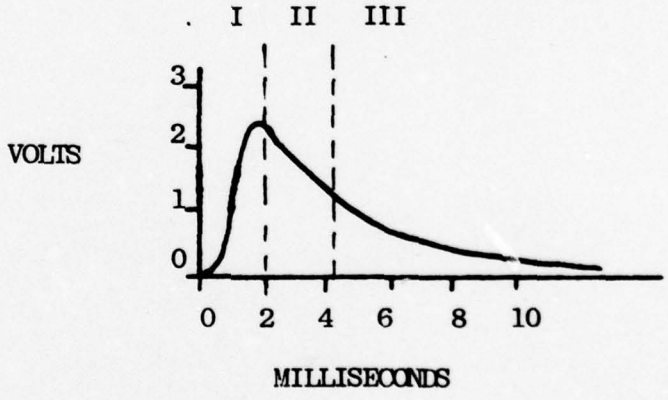

Figure 10. Output Pulse of the Superconducting Pulse Generator with a 40Ω and .7 mH Load.

results from the separate layers of heater and superconducting wire in the thermal switch which was necessitated by the fragility of the superconductor's insulation causing shorts in the switch during construction. An uniform interweaving of the two types of wire with the superconductor forming a bifilar was the preferred design but could not be constructed with the materials and techniques available.

With the nonsquare pulses produced in the experiment, direct detailed comparison of the generator's performance into the various loads was not possible. Indirect comparison of the results can be made of the pulses produced as shown in Figure 10. The pulse can be analyzed by dividing it into three sections as shown in the diagram. The rising edge is due to the slow rise in the resistance of the output switch into which approximately 30% of the pulse's energy is lost and the line current is reduced during this period also by 30%. The second section, which is approximately 2 milliseconds in length, is a reflected wave generated by the changing resistance in the first period producing a straight line in the second section. The final section is the exponential tail similar to that produced in the room temperature tests. This section results from a combination of load and output stage mismatch and the nonideal performance of a truncated transmission line model.

The pulse shown in Figure 10 had an efficiency of greater than 60%, if the energy delivered to the output switch is included the efficiency rises to over 90% though the exact figure is unknown. To compare the pulse produced with various loads a wave factor was

defined as the ratio of the voltage across the preceeding inductor to that of the output inductor, given by the equation

$$W.F. = \frac{V_{L5}}{V_{L6}} \tag{13}$$

with the voltages shown in Figure 2 just after the peak of the pulse. At that point in the pulse, the current should be declining uniformly as the magnitude of the reflected wave is falling. A poor match in the load to the line is evidenced by a low wave factor as demonstrated in Figure 11 in which the resistive load is varied from 50% to 200% of the nominal impedance of the line, 33Ω. Note that the best line match was found to be a 40Ω load when data from the peak of the pulse was used because the resistance of the output switch was still low enough to effect the output stage, that is 300Ω in the switch.

In Figure 12 two graphs are shown, the first being the wave factors for 40Ω load with capacitances up to 2.6 times the value of the line capacitance of 5 μfarads in parallel with the 40Ω. The graph II shows the effect of adding in series with the 40Ω load a .7 millihenry inductance which is .14 of the line inductance L_o. These two graphs show by a smaller wave factor as the capacitance in the load is increased that in the later part of the pulse the wave action is reduced by the addition of capacitance to the output stage. The capacitance was introduced to reduce the initial voltage overshoot of 100% from the pulse generator. This turn on spike in

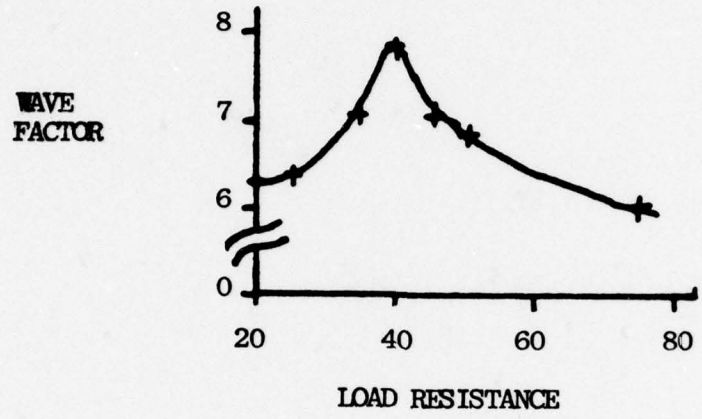

Figure 11. Output Pulse Wave Factor for Various Resistive Loads.

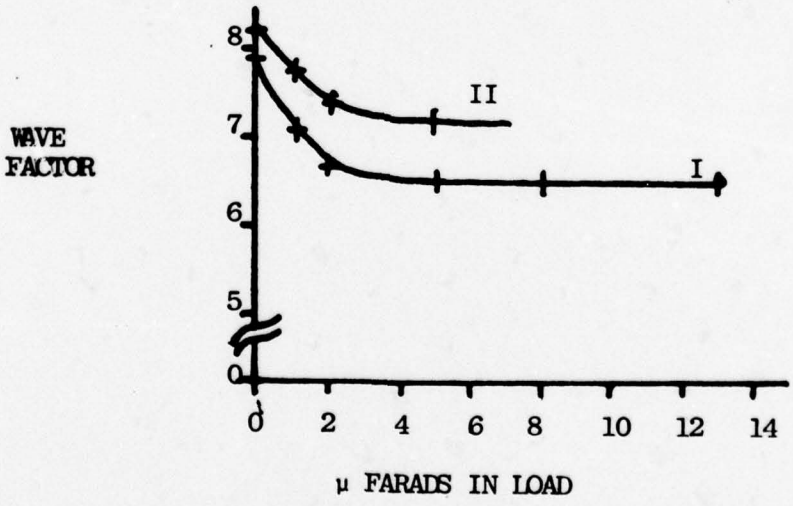

Figure 12. Output Pulse Wave Factor with 40Ω I, and 40Ω + .7 mH, II, for Various Capacitance in the Load.

voltage of the pulse generator could be used to trigger a breakdown in a device in which case no capacitance would be desired in the output stage.

The second point shown by the graphs (Fig. 12) is that a partially inductive load, if the inductance of the load is small compared to the line inductors, does not seriously degrade the wave action or efficiency of the line. An oscillogram is shown in Figure 13 that is typical of the type used to determine the wave factors. The three traces in the figure are the voltage of the load, top; the voltage of capacitor C_5, middle; and the voltage of capacitor C_4, bottom, from which the voltages across L_6 and L_5 are determined. The peaks in Figure 13 are displaced in time with the expected displacement of 1.6×10^{-4} seconds per section for propagation of a signal along the line.

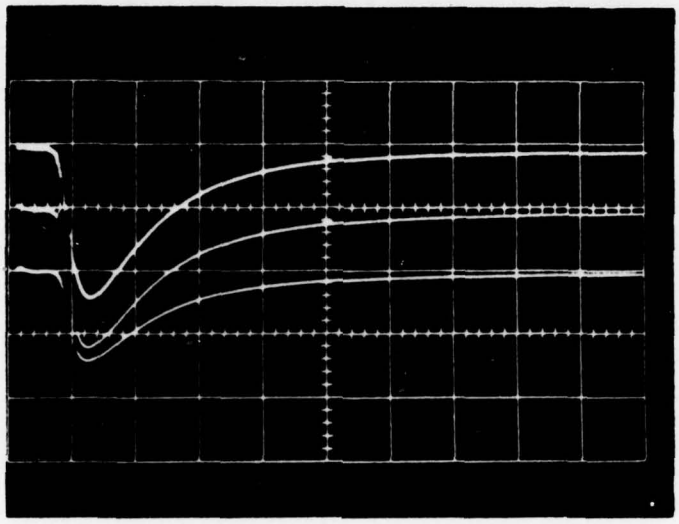

Figure 13. Oscillogram of the Superconducting Pulse Generator Output.

CHAPTER III

FLUX PUMP

1. General Considerations

To charge the inductors of the pulse generator a discrete component flux pump based on the design of Laquer[13] was constructed. The pump as shown in the Figure 14 operates in the following sequence;

1) With switches S1 and S2 closed flux is introduced to the transformer by an externally sourced current in the primary coil.

2) Both switches S1 and S2 are closed forming a superconducting loop in the secondary in which the transformer flux is trapped.

3) The external current in the primary is reduced to zero or reversed inducing a current in the secondary such that flux in the superconducting secondary loop is conserved.

4) Switch S2 is opened causing a redistribution of flux between the secondary coil and the storage coil.

If the current induced in the secondary in step 3 exceeds the current in the storage coil, the current established in both the secondary and storage coils in step 4 will be greater than the initial current of the storage coil. Thus current or its related magnetic flux is pumped into the storage coil by this device.

Since the development by Laquer, numerous models have been

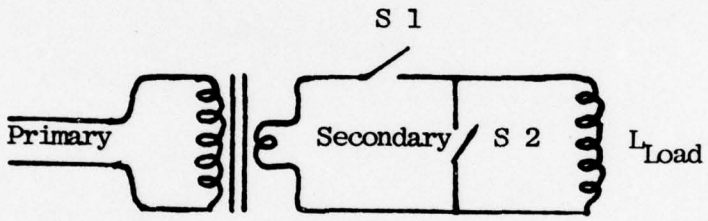

Figure 14. Basic Discrete Component Flux Pump Schematic.

built[18-20] including publications detailing the controlling electronics.[21] However most of these flux pumps cycled at slow rates and used thermal switches.[18,19] The flux pump for this project was designed for high speed cycling, up to several kilohertz. To obtain high cycling rates magnetic switches were required and a core of high magnetic permeability was used in the switches to reduce the current needed for generation of a critical field.

The advantage of the high cycling speeds is that for a given size of transform, with the saturation magnetic field of the transformer limiting the maximum energy transferred per cycle, more power can flow through the flux pump. If the cycling speed is sufficiently high, a superconducting storage coil or magnet can be charged directly from alternating current power sources at 60 or 400 hertz, for example. This can greatly simplify the power supply requirements for a superconducting system as only controlling electronics for the switches is needed external to the cryostat with no rectification of the power into flux pump.

2. Flux Pump Built

A diagram of the flux pump built with schematic specifications is shown in Figure 15. The first of the two major components of the flux pump is the transformer. The superconducting switches will be discussed second and the controlling electronics are

treated in the following chapter.

The choice of material for the transformer core is a trade off of relative permeability (μ_r) and saturation magnetic field (B_s). A high B_s yields a large number of ampere turns for saturation given by

$$NI = \frac{B_s 2\pi r}{\mu_o \mu_r} \text{ ampere turns} \qquad (14)$$

for a toroid of radius r. The materials such as iron which have a high B_s also have high μ_r which reduces the ampere turns needed for a given field. The choice of pure nickel was made because nickel has a low μ_r equal to 50 versus iron's 4,000 with B_s of .6 tesla for nickel versus 2 tesla for iron. The advantage of a nickel core in high current applications can be shown by the saturation ampere turns of a core of 5 centimeters nominal radius. Using Eq. (14) a comparison of nickel and iron cores gives

Nickel - 3×10^3 ampere turns,

Iron - 1.2×10^2 ampere turns.

The transformers built from nickel will have a larger leakage flux than iron core transformers because the μ_r of the nickel is only 1% that of the iron.

For use in the flux pump, the high frequency limit of the transformer, which is controlled by the induced eddy currents, must be above the operating frequency of the pump. Therefore, the core was constructed of .61 millimeter diameter nickel wire with epoxy between the turns. The frequency limit can be estimated

as the frequency that yields a skin depth equal to the radius of the wire used. This calculation is made using the equation

$$f = \frac{1}{\delta^2 \pi \mu \sigma} \tag{15}$$

where f is the frequency, δ is the skin depth, μ is the magnetic permeability and σ is the electrical conductivity of the material. For the nickel wire used, the limiting frequency is on the order of 10^5 hertz.

The transformer core was constructed by winding one continuous length of .61 millimeter diameter wire with epoxy interlacing. The primary and secondary coils were threaded through the center of the core with the primary of 200 turns and the secondary of 2 turns both of multifilamentry niobium-titanium wire.

The design of the two switches in the flux pump was based on the application of a magnetic field to a type I superconductor. Niobium was chosen for its critical field of .2 tesla and electrical resistivity at the cryogenic temperatures of $.5 \times 10^{-8} \Omega$-meters. A Mumetal core was used in the switches with the niobium foil positioned in a 1 millimeter gap to reduce the magnetic reluctance of the switch and thus the power supply requirements to generate the critical magnetic field to switch the niobium into the normal state. With a relative permeability of 20,000 for Mumetal, all the reluctance in the switches comes from the air gap in which the niobium foil was placed. For a 1 millimeter gap, the required magnetic field of .2 tesla is obtained with

$$NI = \frac{B\ell}{\mu_o} \quad \text{ampere turns} \tag{16}$$

where ℓ is the length of the gap. Numerically 150 ampere turns is needed for switching compared with over 10^3 ampere turns for an air core switch.

The high frequency operation of the switch can be limited by the eddy currents induced in the core material limiting the penetration rate of magnetic flux. The Mumetal used was in sheets .4 millimeters thick, as the Mumetal has an electrical conductivity lower than nickel, the limiting frequency of the Mumetal core will be higher than that of the transformer whose needed penetration depth is greater.

The second possible limit on the switching rate was the power supply used to drive the switches. The rise in current of the switch coil was limited by

$$\frac{dI}{dt} = \frac{V}{L} \tag{17}$$

where V is the power supply voltage and L is the inductance of the switch coil. For the switches built, the rate of current rise was limited to 10^3 amperes per second. This will establish the maximum frequency of the switches and the flux pump at

$$F_{ST} \leq \frac{10^3}{I_s} \quad \text{hertz} \tag{18}$$

where I_s is the current needed to exceed the niobium critical

magnetic field and F_{ST} is the frequency at which the flux pump is stepped through the states listed in section 3.1.

The switches were constructed by rolling 2 centimeter wide strips of Mumetal on a 1.5 centimeter former with epoxy between each layer. The hardened core was cut to form a gap into which a double layer of 1.3×10^{-5} meter thick niobium foil was placed. The foil was spot welded to the multifilamentry niobium-titanium wire used in the flux pump. Then the gap was compressed by a threaded brass rod through the switch core to yield a minimum gap with a uniform magnetic field.

The dimensions of the niobium foil were chosen to yield a critical current greater than 20 amperes. This high secondary current was needed because the low inductance in the flux pump secondary, less than .5 μhenries, requires a high current in the secondary to store and transfer a reasonable amount of energy in one cycle. For 10 amperes in the secondary there is an energy of 10^{-5} joules compared with the energy in the pulse generator at one ampere of 10^{-2} joules. The normal state of the niobium foil was $5 \times 10^{-3}\Omega$ yielding a time constant for the secondary of under 10^{-4} seconds which equals the minimum stepping time of the flux pump.

3. Experimental Performance

The flux pump constructed was operated and did perform according to the theory derived by Laquer[13] with high frequency fall off of efficiency beginning at the expected stepping frequency of 4 kilohertz. Two problems effected the experimental results;

first, the low coupling of the nickel transformer to the two turn secondary of less than 20%, which yielded an energy transfer efficiency under 4%; secondly, the spot welds used in connecting the niobium foil switches introduced a total of 50μΩ, limited the secondary critical current to 2 amperes and reduced the current established in the secondary upon reduction of current in the primary, as a fully superconducting loop was not established in the secondary.

The low coupling coefficient of the transformer was expected from room temperature tests with a six turn secondary having 40% coupling. This same test verified the transform action up to 40 kilohertz with the secondary open circuit voltage undiminished. The low coupling rendered calculations of the efficiency of the flux pump, based on energy into the primary, useless as they yielded results that were less than 3% even at the most efficient cycling rates.

With a total secondary loop inductance of .3 μhenries and 50μΩ in the spot welds of the switches, a time constant for the current in the secondary of 6 milliseconds is obtained. This results in a significant loss of flux in the secondary before the S2 switch opens and flux is redistributed between the secondary and storage coils at the lower cycling frequencies. A graph of the normalized efficiency of the flux pump versus stepping frequency is shown in Figure 16, which shows the decline in efficiency at low frequencies due to the 50μΩ.

The currents needed to operate the switches were found to be

.25 amperes resulting from the gaps in the switches being set as small as nonuniformities in the surfaces would allow. These current levels resulted in the high frequency fall off in efficiency of the flux pump shown in Fig. 16 being 4 kilohertz as expected by Eq. (18). Overdriving the switches to a current 50% higher than the value needed for static operation increased the high frequency efficiency of the flux pump as full power supply voltage was maintained on the switch coils until after the current was above that needed for switching.

The decline in pump efficiency with the number of cycles run is plotted in Figure 17 and is compared in Appendix A with that predicted by Laquer. The agreement shown in Appendix A between theory and experimental results, when the effect of the 50μΩ is allowed for, helps to verify the proper operation of the flux pump.

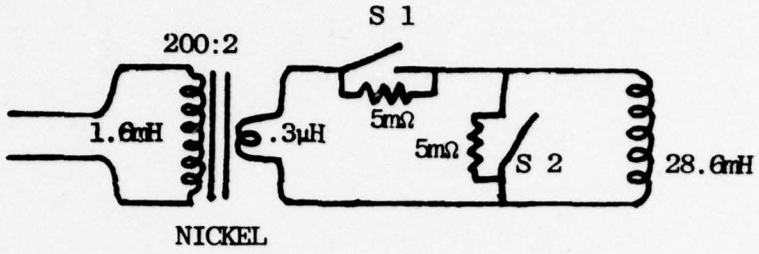

Figure 15. Schematic of Flux Pump Used in the Pulsed Power Supply.

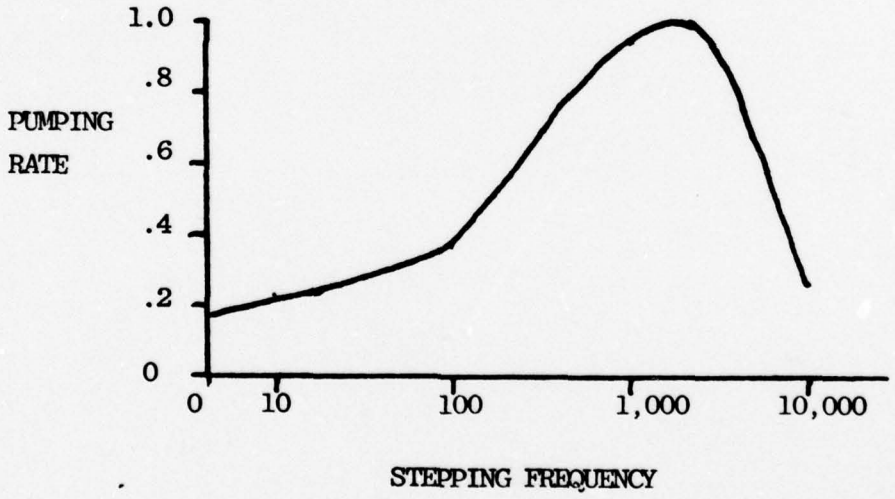

Figure 16. Normalized Efficiency of the Flux Pump versus Stepping Frequency.

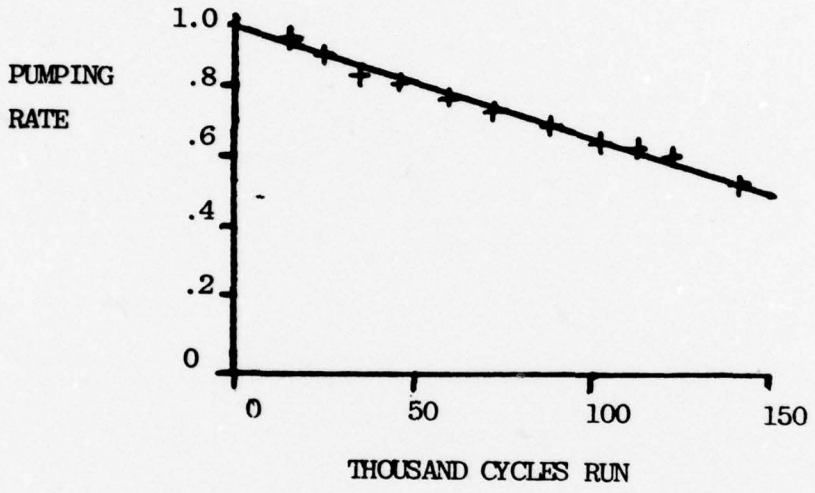

Figure 17. Normalized Cumulative Pumping Rate of the Flux Pump Versus the Number of Pumping Cycles Executed.

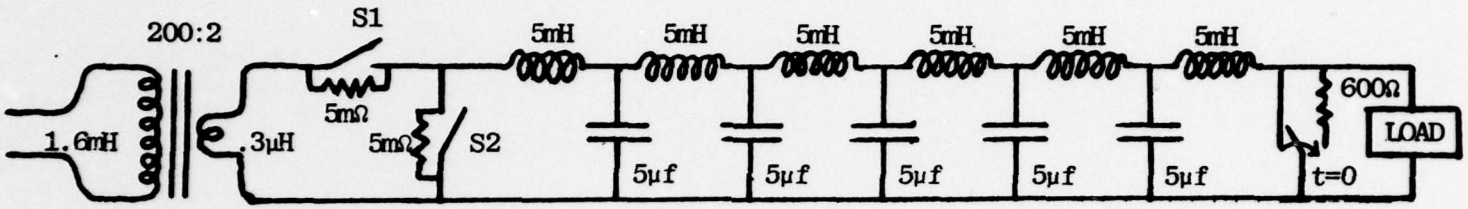

Figure 18. Schematic of the Pulsed Power Supply.

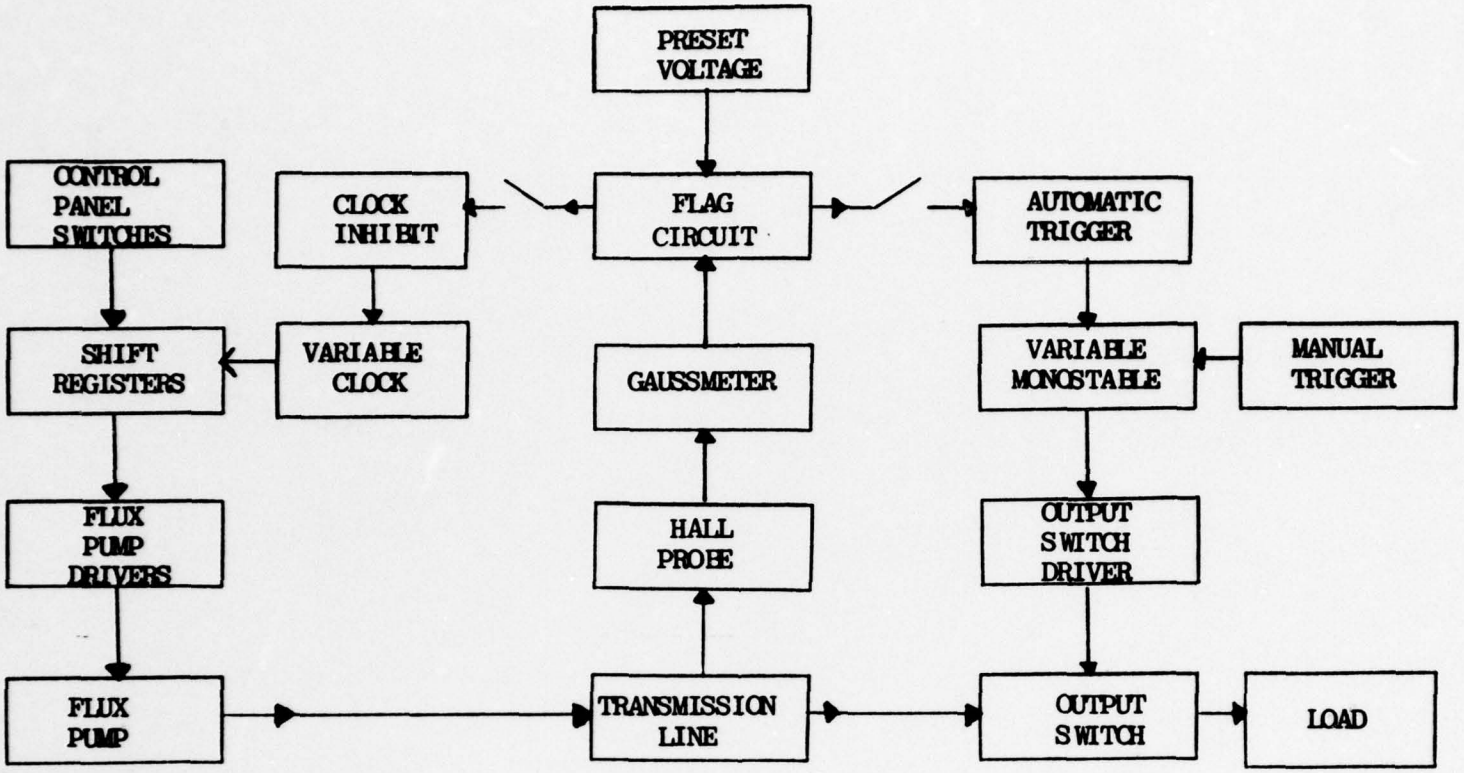

Figure 19. Flow Diagram of the Electronic Control System of the Pulsed Power Supply.

CHAPTER IV

EXPERIMENTAL SYSTEM

The two major parts of the pulsed power supply, the pulse generator and flux pump, were interconnected as shown in Figure 18. To operate the pulse generator, an electronic control system including driver circuits was constructed. The control system had three basic functions; first, to operate the flux pump to charge the storage indcutors; second, to open the output switch of the pulse generator; third, to determine the current in the inductors and use this information to initiate the other two functions. A flow diagram of the control system is shown in Figure 19.

The control of the flux pump was designed to be flexible by use of a variable clock driving shift registers whose inputs were switches located on the electronics control panel. The serial output of the shift registers was used to turn on or off the current in the drivers of the transformer and the two magnetic switches of the flux pump. All the driver circuits, including the one for the pulse generator switch, had adjustable currents with the value of the voltages and currents of the driven devices available. In the case of the transformer a reverse demagnetizing current was optionally available.

The driver circuit which opened the pulse generator switch was a variable monostable controlled current source that was triggered manually with a push button or by the automatic system. The automatic

system, when engaged, started and stopped the flux pump and opened or closed the pulse generator switch depending on the current level inside the storage coils as determined by a hall probe located in one of the coils and connected to a digital gauss meter. The analog voltage output of the gauss meter was compared to a preset voltage level and if it was higher than the preset voltage, the flag circuit's output was set to its high state. The flag was a signal available to stop the flux pump, trigger the pulse generator or a combination of both when its output was in the high state.

The outputs obtained from the pulse generator and used as data in Chapter II made use of the fully automatic operation of the pulsed power supply. The flux pump was operated at a 2 kilohertz stepping frequency until a current of .1 amperes was obtained in the storage coils whereupon a pulse was generated and the process repeated. For data used in Chapter III on the flux pump, no pulse was generated; the flux pump was driven until the preset current level was reached and then stopped.

The driver circuit's final stages were darlington transistors limited to 1 or 2 amperes in the different circuits and capable of allowing a 10 volt drop across the coils or heater. This voltage formed the limit of the charging speed of the flux pump switches at 10^3 amperes per second and limited the thermal switch power to 10 watts. The gating electronics and shift registers were C-Mos digital components using the same power supply as the driver circuits. An FET op-amp, to reduce loading effects on the gauss meter, was used in

the flag circuit to compare the current level in the pulse generator to the preset level.

The superconducting experiment was conducted in a .1 meter diameter glass dewar with a vacuum jacket. Surrounding the experiment was radiation shielding and liquid nitrogen filled shields. This allowed running the experiment for up to five hours after filling with liquid helium. Precooling before filling with liquid helium was done by a combination of radiation and convective cooling from the liquid nitrogen filled shields.

CHAPTER V

CONCLUSION AND DISCUSSIONS

1. Discussion of Results

The first objective of this project, to demonstrate high efficiency in pulse generation from superconducting inductors with one switch and all passive components, was realized. An efficiency of over 60% to the load was shown with the output thermal switch reducing this value from the near 100% efficiency demonstrated in the room temperature version of the pulse generator. It was also shown that modification of the edges of the pulse is possible by varying the components in the output stage of the generator. The transmission line scheme used as discussed and demonstrated experimentally retained high efficiency over a variety of loads including inductive loads.

The main disadvantage to this approach of pulse generation is the large amount of capacitance needed to implement the design. Equal amounts of energy storage capacity are required of the inductors and of the capacitors; however, only the inductors initially store energy. The result is a 50% utilization of the energy storage capacity of the line, which is compensated for by the increased efficiency of pulse generation for certain load requirements. Under those conditions discussed in section 2.3, the pulsed power supply, including energy source, based on the transmission line scheme can be more economical than a single inductor storage and discharge scheme. Specifications on the load requirements and constraints on the energy source must be

known for a design choice between the two schemes.

The use of the system built with an improved output switch offers versatile design parameters of output current, voltage and power. Superconducting wires offer the possibility of currents up to hundreds of kiloamperes and work is being done on handling voltages in the hundred kilovolt range inside the cryogenic environment.

The flux pump built for this project adds one new feature to the list of advantages of a discrete flux pump, which includes small current leads and generation of high current, over direct charging of superconducting coils; the new feature is high speed cycling. The transformer of this flux pump could be run directly from alternating current sources of up to 2 kilohertz with only timing circuitry for control of the switches external to the cryostat. The construction of this type of flux pump for slow cycling speeds was discussed in detail by Bernat et al.[21] whose pump includes a two inductor secondary system.

2. Work to be Done

The most needed improvement to this system is the construction of a faster acting output switch. The flux pump switches switched cleanly when turned on and off at 10 kilohertz; however, their low normal state resistance, 5mΩ, makes them inapplicable for the output switch. Also a better method of joining the niobium foil to the superconducting wire to reduce the resistance of the joint below the μohm range is needed for the flux pump switches to form better superconducting loops. As stated earlier, a promising prospect for high

impedance magnetic switches may lie in thin films on which much work is being done.[22-27] These references give an introduction to the many and varied problems that will be encountered in development of thin film magnetic switches.

The second major area to be studied is the design of the pulse generator line. This, to identify and test more options in the trade off of capacity utilization and energy transfer efficiency, such as tapered lines of the form of time limited filters.[28] Or, to make modifications in the line that would change the shape of the pulse by use of different inductor-capacitor relations and arrangements than the transmission line scheme.

REFERENCES

1. Kolm, H. H., "The Future of Superconducting Technology", Cryogenics, Vol. 15, No. 2, pp. 63, 1975.

2. Brimingham, B. W. and Smith, C. N., "A Survey of Large Scale Applications of Superconductivity in the U.S.", Cryogenics, Vol. 16, No. 2, pp. 59, 1976.

3. Gilbert, W. S., "Summary of International Progress on Superconducting Magnets", IEEE Transactions on Nuclear Science, Vol. NS 20, No. 3, pp. 668, 1973.

4. Malkov, M. P. and Sytchev, V. V., "Soviet Research in Cryogenics, Vol. 15, No. 2, pp. 65, 1975.

5. Laquer, H. L., "Superconducting Magnetic Energy Storage", Cryogenics, Vol. 15, No. 2, pp. 73, 1975.

6. Boom, R. W., Mohan, N. and Peterson, H. A., "Superconductive Energy Storage Inductor - Converter Units for Power Systems", IEEE Transactions on Power Apparatus and Systems, Vol. PAS-94, No. 4, pp. 1337, 1975.

7. Swannack, C. E., et al., "10kA, 300 kJ Magnetic Energy Transfer and Storage (METS) Test Facility", IEEE Transactions on Magnetics, Vol. MAG-11, No. 2, pp. 504, 1975.

8. Punchard, W. F. B., "A 300 kJ Pulsed Superconducting Energy Storage Coil", IEEE Transactions on Magnetics, Vol. MAG-11, No. 2, pp. 508, 1975.

9. Cowan, M., Cnare, E. C., Leisher, W. B., Tucker, W. K., and Wesanberg, D. L., "Pulsed Energy Conversion with a DC Superconducting Magnet", Cryogenics, Vol. 16, No. 12, pp. 699, 1976.

10 Honig, E. M., Swannack, C. E. Warren, R. W., and Whitaker, D.H., "Progress in Switching Technology for METS System", IEEE Transactions on Plasma Science, Vol. PS-5, No. 2, pp. 61, 1977.

11. Mawardi, O. K., "Proposal on the Pulsed Superconductive Shaping Circuit", submitted to USAF Office of Scientific Research, April, 1977.

12. Vinogradov, A. A., Goncharov, V. A., Levitov, V. I., and Starobinskii, V. Ya., "High Voltage Cryostats for 120 and 220kV", Cryogenics, Vol. 15, No. 4, pp. 225, 1975.

13. Laquer, H. L., "An Electrical Flux Pump for Powering Superconducting Magnet Coils", Cryogenics, Vol. 3, No. 2, pp. 27, 1963.

14. Hayt, W. H., "Engineering Electromagnetics", McGraw-Hill; New York, pp. 407, 1974.

15. Stekly, Z. J. J. and Thome, R. J., "Large-Scale Applications of Superconducting Coils", Proceedings of the IEEE, Vol. 61, No. 1, pp. 85, 1973.

16. Cresenzo, E. Di., Indovina, P. L., Onori, S. and Rogani, A., "Temperature and Thickness Dependence of Critical Magnetic Fields in Lead Superconducting Films", Physical Review B, Vol. 7, No. 7, pp. 3058, 1973.

17. Isaac, R. D. and Schwarz, R. B., "Simple Persistent Switch for Superconducting Solenoids", Review of Scientific Instrumentation, Vol. 46, No. 5, pp. 638, 1975.

18. Homer, G. J., Houzego, P. J., Scott, C. A. and Wilson, M. N., "A Thermally Switched Flux Pump", IEEE Transactions on Magnetics", Vol. MAG-11, No. 2, pp. 576, 1975.

19. Droege, T. G., Purcell, J. R. and Wang, S. T., "A Slow Cycling Flux Pump Using Digital Control", IEEE Transactions on Magnetics, Vol. MAG-11, No. 2, pp. 580, 1975.

20. Carroll, K. J., "Behavior of a Flux Pump Using an Automatic Superconducting Switch", Cryogenics, Vol. 13, No. 6, pp. 353, 1973.

21. Bernat, T. P., Blair, D. G. and Hamilton, W. O., "Automated Flux Pump for Energizing High Current Superconducting Loads", Review of Scientific Instrumentation, Vol. 46, No. 5, pp. 582, 1975.

22. Grawatsch, K., Kofler, H., Komarek, P., Kormann, H. and Ulbricht, A., "Investigations for the Development of Superconducting Power Switches", IEEE Transactions on Magnetics, Vol. MAG-11, No. 2, pp. 586, 1975.

23. Wolf, S. A., Kennedy, J. J. and Nisenoff, M., "Properties of Superconducting RF Sputtered Ultrathin Films of Nb", Journal of Vacuum Science and Technology, Vol. 13, No. 1, pp. 145, 1976.

24. Heubener, R. P., Kampwirth, R. T. ,Martin, R. L., Barbee, T. W. and Zubeck, R. B., "Critical Current Density in Superconducting Niobium Films", IEEE Transactions on Magnetics, Vol. MAG-11, No. 2, pp. 344, 1975.

25. Eru, I. I., Komashko, V. A., Krut'ko, A. P., Peskovatskii, S. A. and Poladich, A. V., "Voltage-Current Curves of Long Superconducting Niobium Films", Soviet Physics-Solid State, Vol. 17, No. 10, pp. 2068, 1976.

26. Anayama, T. and Saito, Y., "The Effects of the Substrate Temperature on Sputter-Deposited Niobium Films", Journal of Low Temperature Physics, Vol. 21, Nos. 1/2, pp. 169, 1975.

27. Crow, J. E. and Strongin, M., "Influence of Normal-State Electrical Resistance on the Superconducting Transition Temperature of Ultrathin Films", Physical Review B, Vol. 3, No. 7, pp. 2365, 1971.

28. Hazony, D. and Hazony, Y. "Time Limited RLC Networks", Proceedings of the Fifteenth Annual Allerton Conference on Communication, Control, and Computing, pp. 642, Monticello, Illinois, 1977.

APPENDIX A

Comparison of Experimental and Calculated Pumping Rates

From Laquer's analysis of the discrete flux pump[13] the flux established in the storage coil after one cycle will be

$$\Phi'_{Load} = Ax \tag{19}$$

where

$$A = I_{secondary} L_{secondary} \tag{20}$$

just after reduction of primary current and

$$x = \frac{L_{Load}}{L_{secondary}+L_{Load}} \tag{21}$$

with subscripts referenced to Figure 14. After the second pumping cycle the flux is

$$\Phi''_{Load} = A(x+x^2) \tag{22}$$

and after n cycles

$$\Phi^n_{Load} = A\left(\frac{x-x^n}{1-x}\right) . \tag{23}$$

To compare the theory with the data used in Figure 17, calculation of Φ_{Load} for two of the data points and comparison of the normalized pumping rates with that of the experiment is made. For the flux pump built the value of x is

$$x = \frac{28.6\ mH}{28.6\ mH + .3\mu H} = .9999895\ . \tag{24}$$

The two data points used were at 7911 and 16,082 cycles with the relative pumping rate given by

$$\frac{\Phi_{Load}^{n_2}\ n_1}{\Phi_{Load}^{n_1}\ n_2} = \frac{(x-x^{n_2+1})n_1}{(x-x^{n_1+1})n_2} \tag{25}$$

and the calculated relative pumping rate equal to .96. This compares with the experimental rate of .94; however, the current lost due to the flux pump switch spot welds must be accounted for in a comparison. Between the two data points was 32 seconds of pumping with the average time constant

$$\tau = \frac{28.6\ mH}{15\mu\Omega} = 1.9 \times 10^3 \text{ seconds} \tag{26}$$

yielding a 2% drop in current. Thus the experimental and calculated relative pumping rates agree with the 2% drop in current during the pumping.